

“ INTEGRATION OF GEOLOGICAL AND GEOPHYSICAL DATA FOR RE-EVALUATION OF LOCAL SEISMIC HAZARD AND GEOLOGICAL STRUCTURE: THE CASE STUDY OF ROMETTA, SICILY (ITALY) ”

Paolo Pino¹, Sebastiano D'Amico², Barbara Orecchio¹, Debora Presti¹, Silvia Scolaro^{1,*}, Antonino Torre¹, Cristina Totaro¹, Daniela Farrugia², Giancarlo Neri¹

⁽¹⁾Department of Mathematics, Computer Sciences, Physics, and Earth Sciences, University of Messina, Messina, Italy

⁽²⁾Department of Geosciences, University of Malta, Malta

Article history

Received November 26, 2016; accepted December 22, 2017.

Subject classification:

Ambient noise; H/V; Seismic array; Site effects.

ABSTRACT

The village of Rometta, northern-eastern Sicily (Southern Italy), experienced severe damage during the most energetic earthquakes that occurred in eastern Sicily and southern Calabria in the last centuries. Geological maps indicate that Rometta primarily lies on a stiff plate of Upper Pliocene - Lower Pleistocene calcarenites and only to minor extent on Middle Pleistocene overlying clays. Rometta represents an interesting case study for site response investigation because of the apparent mismatch between the currently available geological knowledge and the level of damage caused by historical seismic events. The local seismic response has been investigated through a grid of 64 single-station measurements of ambient seismic noise by the Horizontal to Vertical Noise Spectral Ratio technique (H/V). Also, phase velocity dispersion curves from seismic array through the Extended Spatial Auto-Correlation method were analyzed. The H/V curves obtained show a ubiquitous frequency peak between 0.5 Hz and 0.9 Hz due to the deep interface between the metamorphic substrate and sedimentary sequence, and a secondary peak in the 2.5-15 Hz interval in most of the measurement points that may be related to a larger extent of the clay outcrops with respect to what is already known from geological investigations. Joint inversion of dispersion and H/V curves was also performed in order to obtain the velocity profile. Results acquired through the combined use of geophysical methods furnished useful information for seismic hazard evaluation where surface geology is not clearly visible because of urbanization and vegetation cover, thus suggesting that a wide extent of clays may reasonably be the cause of past earthquake damage distribution.

1. INTRODUCTION

The village of Rometta is located in NE Sicily (Figure 1), within a segment of the Neogene Apennine-Maghrebide orogenic belt, which developed in the Central Mediterranean Sea as a result of collision between Africa and Europe and northwesterly subduction and roll-back of the Ionian slab [Ghisetti and Vezzani, 1982; Malinverno and Ryan, 1986]. North-eastern Sicily presently separates the Tyrrhenian basin (to the NW) and the Ionian basin (to the SE), both representing back-arc areas [Gueguen et al., 1997; Faccenna et al., 2001].

Rometta experienced severe damage during the strongest historical earthquakes (for example 11 January 1693, I=XI MCS Mw=7.4; 5 February 1783, I=XI

Mw=7.1; 28 December 1908, I=XI MCS Mw=7.1, Locati et al., [2016]) that occurred in eastern Sicily and southern Calabria [Figure 1; Baratta, 1910; Locati et al., 2016]. Also, macroseismic data (<https://emidius.mi.ingv.it/CPTI15-DBMI15/>) indicates that major earthquake effects in Rometta were frequently greater compared to nearby locations thus leading us to investigate the presence of heterogeneous geological settings potentially able to produce significantly differentiated seismic responses.

A quick estimate of the surface geology effects on seismic motion is provided by the Horizontal to Vertical noise Spectral Ratio (HVSR) technique [Lermo and Chavez-Garcia, 1993; Konno and Ohmachi, 1998; Bard, 1999; Bonnefoy-Claudet, 2006a; D'Amico et al., 2008,

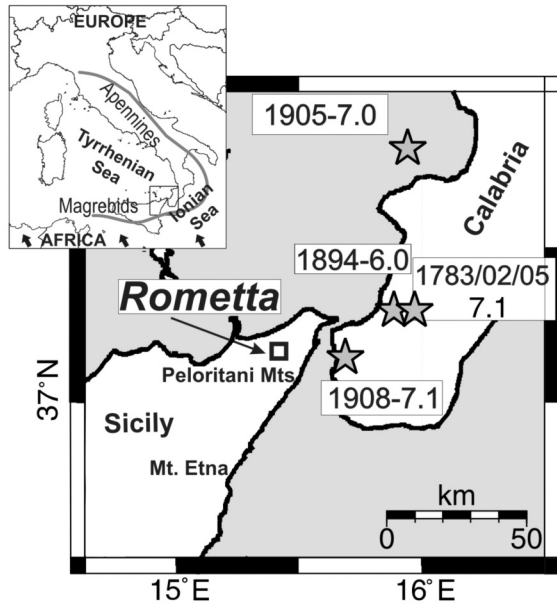


FIGURE 1. The map shows the location of Rometta village, NE Sicily, and the epicenter (stars) of historical events producing effects of least of degree VII (MKS scale; <https://emidius.mi.ingv.it/CPTI15-DBMI15/>) in Rometta. The year of earthquakes occurrence and the relative magnitude are reported. The inset shows the northwestern trending convergence between African and European plates (black arrows) [Calais et al., 2003; Nocquet and Calais, 2004; Nocquet, 2012] and the Apennine-Maghrebides orogenic belt (grey line) [Neri et al., 2009].

Castellaro and Mulargia, 2009; Vella et al. 2013; Paolucci et al., 2015; Scolaro et al., 2018]. This technique relies on the recording and analysis of the environmental ground noise, both of natural and anthropogenic origin, and uses the Fourier amplitude spectral ratio between the horizontal to vertical components of the recorded signals [Nogoshi and Igarashi, 1971; Nakamura, 1989; Bonnefoy-Claudet, 2006a and 2006b]. The basic hypothesis of seismic ambient noise theory is that a resonance peak in the H/V ratio may be interpreted both in terms of SH-wave resonance in superficial layers or in terms of ellipticity if Rayleigh surface waves predominate [Nogoshi and Igarashi, 1971; Lachet and Bard, 1994; Scherbaum et al., 2003]. The wavefield is a combination of both types of waves and then the H/V curve contains information about the shear wave velocity profile in shallow sediments. Also, it is commonly accepted that, although the single components of ambient noise can show large spectral variations as a function of natural and cultural disturbances, the horizontal to vertical noise spectral ratio tends to remain invariant, therefore preserving the fundamental frequency peak [Cara et al., 2003].

In the present study, single-station horizontal to vertical spectral ratio technique (HVSr) and multi-station (seismic array) configurations have been used to determine dynamical properties of the subsoil of Rometta from noise measurements. We performed 64 measurements of ambient noise by using the 3-component Tromino velocimeter (www.tromino.eu), and we estimated shear wave velocity (V_s) profiles by analyzing phase velocity dispersion curves from seismic arrays through the Extended Spatial Auto Correlation (ESAC) method [Ohuri et al., 2002; Okada, 2003; Parolai et al., 2006; Albarello et al., 2011].

Results obtained from measurement analyses, compared with the local geology, furnishes new information useful for seismic risk mitigation.

2. GEOLOGICAL SETTING AND STRATIGRAPHIC FRAMEWORK OF ROMETTA HILL

The main tectonic features of the study area, located in the Peloritani Mts. (Figure 1), is represented by a NE-SW and NNE-SSW oriented normal fault system, which causes brittle deformation of the contractional architecture [Bonini et al., 2011] and controls the actual setting of this sector of the Sicilian Tyrrhenian coast [Guarnieri and Carbone, 2003; Di Stefano et al., 2007]. The extensional tectonic activity of the Peloritani Mts. relates to the opening of the Tyrrhenian Sea and more recently of the Messina Straits [Bonini et al., 2011]. In this area paleozoic high-grade metamorphic rocks outcrop extensively (Aspromonte Nappe, Aut.), locally covered by heterogeneous sedimentary Middle Upper Miocene - Middle Pleistocene successions [Lentini et al., 2000; APAT, 2008].

The landscape of the Peloritani Mts. reflects the tectonic setting of the area, in particular the intense recent dynamics related to strong tectonic uplift [Montenat et al., 1991; Westaway, 1993; Tortorici et al., 1995]. Vertical movements during the late Quaternary controlled the shaping of the landforms as indicated by isolated hills and NW-SE elongated hilly ranges with steep slopes deeply cut by V-shaped valleys, tectonically structured in a half-graben downdropped toward the Tyrrhenian sea.

Rometta hill is surrounded by cliffs and escarpments (Figure 2a). This geomorphological framework clearly shows the sequence of lithological units outcropping (Figure 2, plots a and b), allowing relatively easy field observations for reconstruction of the lateral and vertical distribution, geometries and thicknesses of the pre-Middle Pleistocene. As inferred by geological maps [Lentini et al., 2000; APAT, 2008, see plots 2c, 2d]

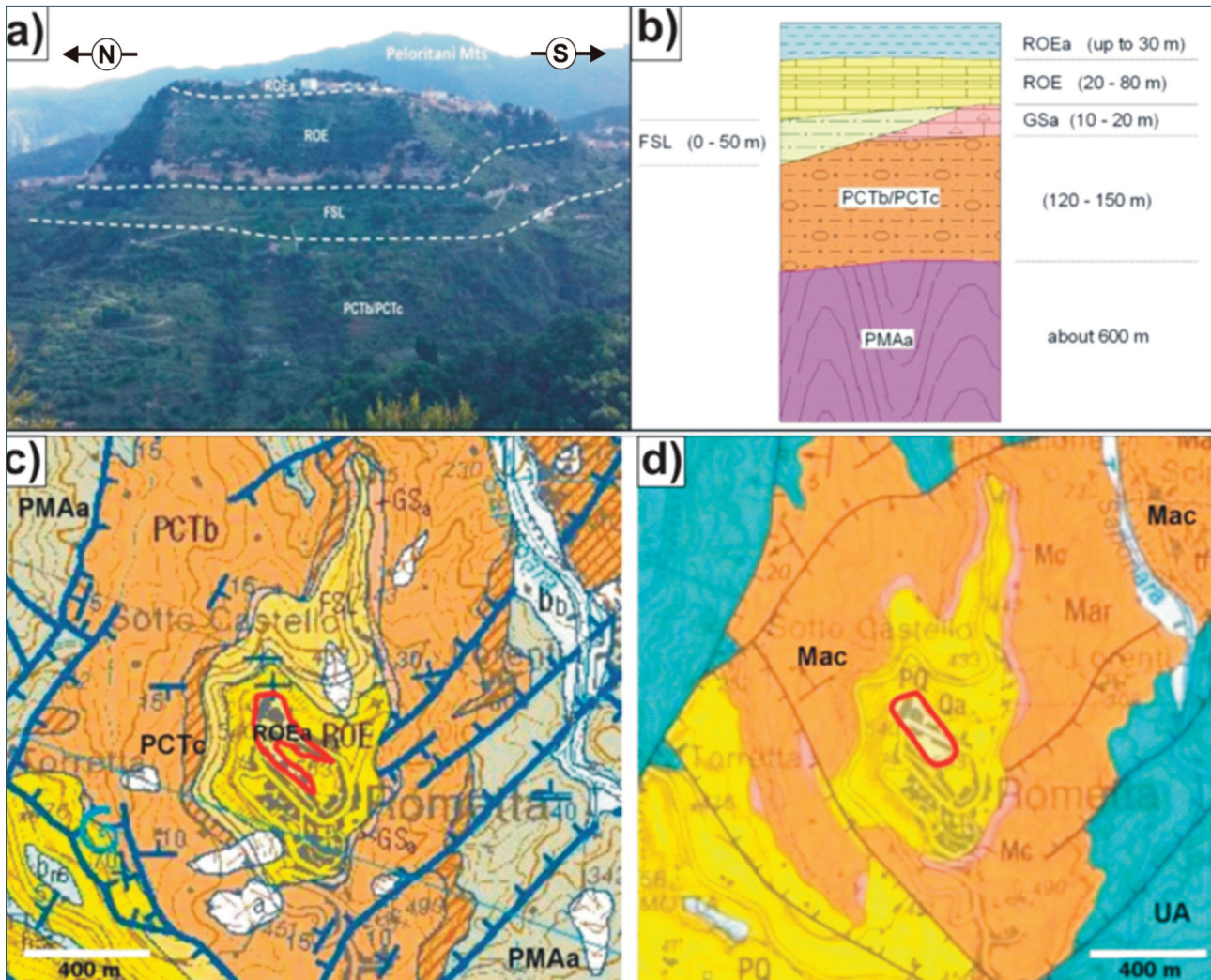


FIGURE 2. (a) Picture of north-western sector of Rometta hill showing abrupt geomorphological framework made of cliffs and steep slopes. Dotted lines illustrate the vertical sharp transition between geological formations. (b) Schematic geological section of Rometta hill. Geological maps of the study area: (c) APAT [2008], (d) Lentini, 2000. Legend: prevailing paragneiss of paleozoic metamorphic Complex - Aspromonte Unit (PMAa and UA); undifferentiated lithofacies of Middle-Upper Miocene San Pier Niceto Formation consisting of well consolidated thick sands and arenites weakly cemented (PCTb and Mar) passing upwards to conglomeratic (PCTc and Mac); stiff upper Messinian evaporitic limestones (GSa and Mc); consolidated and massive Middle Pliocene sandy marls of Massa S. Lucia Formation (FSL); stiff calcarenites massive and cross-stratified of Upper Pliocene - Lower Pleistocene (ROE and PQ) with at the top marly clay Middle Pleistocene (ROEa and Qa) both attributed to Rometta Formation. The latter have been evidenced by red contour.

Rometta village is mainly set on the Upper Pliocene-Lower Pleistocene calcarenites (Rometta Formation Aut.) overlaid by Middle Pleistocene blue marly clays, which are bounded by an erosional unconformity and sedimentary gap [Di Stefano et al., 2007] forming the highest part of the Rometta Hill up to 563 m. a.s.l. (Figure 2).

The calcarenitic unit (ROE in Figure 2c and PQ in Figure 2d) has been considered lithologically articulated [Di Stefano et al., 2007], consisting of alternating different lithofacies, often organized into 1-2 m thick tabular beds, from massive to cross-stratified, rich in bioclastic content, usually poorly cemented. The thicknesses observed are quite variable reaching the maximum in the northern and western urban areas (80 m),

tapering to 10-20 m along the southern rim of Rometta Hill, and are intermediate (40 m) in the eastern areas (Figure 2b). The calcarenitic unit forms a stiff plate from tabular to wedge-shaped (Figure 2b), overlying a diversified sedimentary substrate comprised mostly of Middle Pliocene yellowish to gray-greenish consolidated sandy marls of the Santa Lucia Formation (Auct.). In the southernmost and easternmost sectors (Figure 2) the calcarenitic unit overlies 10-20 m of Messinian tabular limestones evaporites (Calcarea di Base Auct), which are locally covered by a few meters of lens-shaped Lower Pliocene whitish marly limestone (Trubi Formation, Auct). The Middle Pliocene sandy marl unit reaches maximum thickness (50 m) in the northern and western

sectors, wedged southward and eastward between calcarenites and Messinian limestones, with pinch-out closures observed only in the northeastern and southwestern Rometta Hill slopes (see geological sketch maps and schematic cross-section in Figure 2). Pliocene and Messinian units unconformably overlie a Middle-Upper Miocene heterogeneous siliciclastic sequence of the San Pier Niceto Formation (Auct.), that consist in a prevailing massive and poorly cemented silty-sandy conglomerates and arenites weakly cemented, from 120 to 150 m thick (Figure 2c), extending from north-west to east. The foot of Rometta Hill consists of several hundred meters (up to 600 m) of bedrock-like Paleozoic folded metamorphic rocks (Aspromonte Unit Auct.), mainly biotitic schists and gneiss (Figure 2c). The entire sedimentary sequence outcropping along the Rometta hill slopes is preserved within a graben aligned NE-SW and, at least for the pre-Middle Pliocene formations, cut by normal fault systems oriented NE-SW, NW-SE and N-S [Lentini et al., 2000; APAT, 2008; Figure 2].

The true thicknesses and areal extent of the Middle Pleistocene marly clay formation are uncertain, since the lower contact with the calcarenites is not visible [Violanti, 1989], both due to dense urbanization and the intense vegetation cover [Di Stefano et al., 2007]. The marly clays have thicknesses of 15-20 m [Di Stefano et al., 2007] up to about 30 m [Violanti, 1989]. About their spatial distribution at the hilltop of Rometta and the geometric relationships with calcarenites, large discrepancies in interpretation emerge from the most recent geological maps [Lentini et al., 2000; APAT, 2008; Figure 2]. In particular, it is not clear which part of the Rometta subsurface is clays or calcarenites.

3. METHODS AND DATA PROCESSING

3.1 SINGLE-STATION H/V MEASUREMENTS

The Horizontal to Vertical Spectral Ratio (H/V) technique for site effects investigation [Nogoshi and Igarashi, 1971; Nakamura 1989 and 1996] was applied in the area of Rometta. This technique consists in estimating the ratio of horizontal and vertical components of the ambient noise spectra recorded at the surface. The spectral ratio reveals a peak corresponding to the fundamental frequency of a site [Bonnetfoy-Claudet et al., 2006a] and the presence of this peak is more accentuated when a sharp impedance contrast exists between low shear-wave velocity layers and the bedrock [Malischewsky and Scherbaum, 2004]. The ambient noise wavefield is a combination of both body and surface waves and the resonance peak can be interpreted both in terms of SH

resonance in superficial layers and of ellipticity if Rayleigh surface waves predominate [Fäh et al., 2001; Scherbaum et al., 2003; Bonnetfoy-Claudet et al., 2006a]. Also, the final H/V curve contains useful information about the relationship between the shear-wave velocity profile of the sedimentary layers and their thickness [Scherbaum et al., 2003].

An extensive survey of single-station ambient noise recordings was carried out in Rometta in order to assess the fundamental resonance frequency of the sedimentary layers. Ambient noise measurements were acquired at 64 points (Figure 3, see also the supplementary material) through the portable seismometer Micromed Tromino (www.tromino.eu). The Tromino is a compact, battery-operated, all-in-one system composed of three orthogonal velocity sensors and 24-bit digitizer, whose sampling frequency extends up to 1024 Hz. Time series of 20 minutes each were recorded at a sampling rate of 256 Hz and data analysis was performed by using the Grilla software (www.tromino.eu). Following the criteria suggested by the SESAME European Project [Bard, 2005], the recorded signals were divided into non-overlapping time windows of 20 s. The Fourier spectrum of each window was calculated and smoothed through a triangular window with frequency dependent half-width (5% of the central frequency). The H/V spectral component ratio was computed for each frequency by averaging the horizontal spectra using the geometrical mean and dividing them by the vertical spectrum for each time window. Before interpreting the resulting curves, we identified and discarded spurious noise windows associated with very close sources (e.g. due to impulsive or strongly localized anthropogenic sources) so that the standard deviation is minimized. Finally, only maxima lying in the frequency range of interest for seismic microzonation and earthquake engineering (i.e. 0.5 - 20 Hz) were taken into account. If final curves showed a single peak, the corresponding frequency (F_0) was considered as the fundamental resonance frequency at the site. If a higher frequency peak was present, it was interpreted as a resonance frequency (F_1) associated with a shallower impedance contrast.

3.2 SEISMIC ARRAY MEASUREMENTS

The Micromed SoilSpy Rosina™ seismic digital acquisition system was used to conduct the passive seismic array measurements. A total of 42 vertical geophones (4.5 Hz) were used. These were placed in an L-shaped configuration (Figure 3) with a regular interstation distance of 5 m. The recordings taken were 20 minutes long, sampled at 256 Hz and finally analyzed using the ESAC technique [Ohuri et al.,

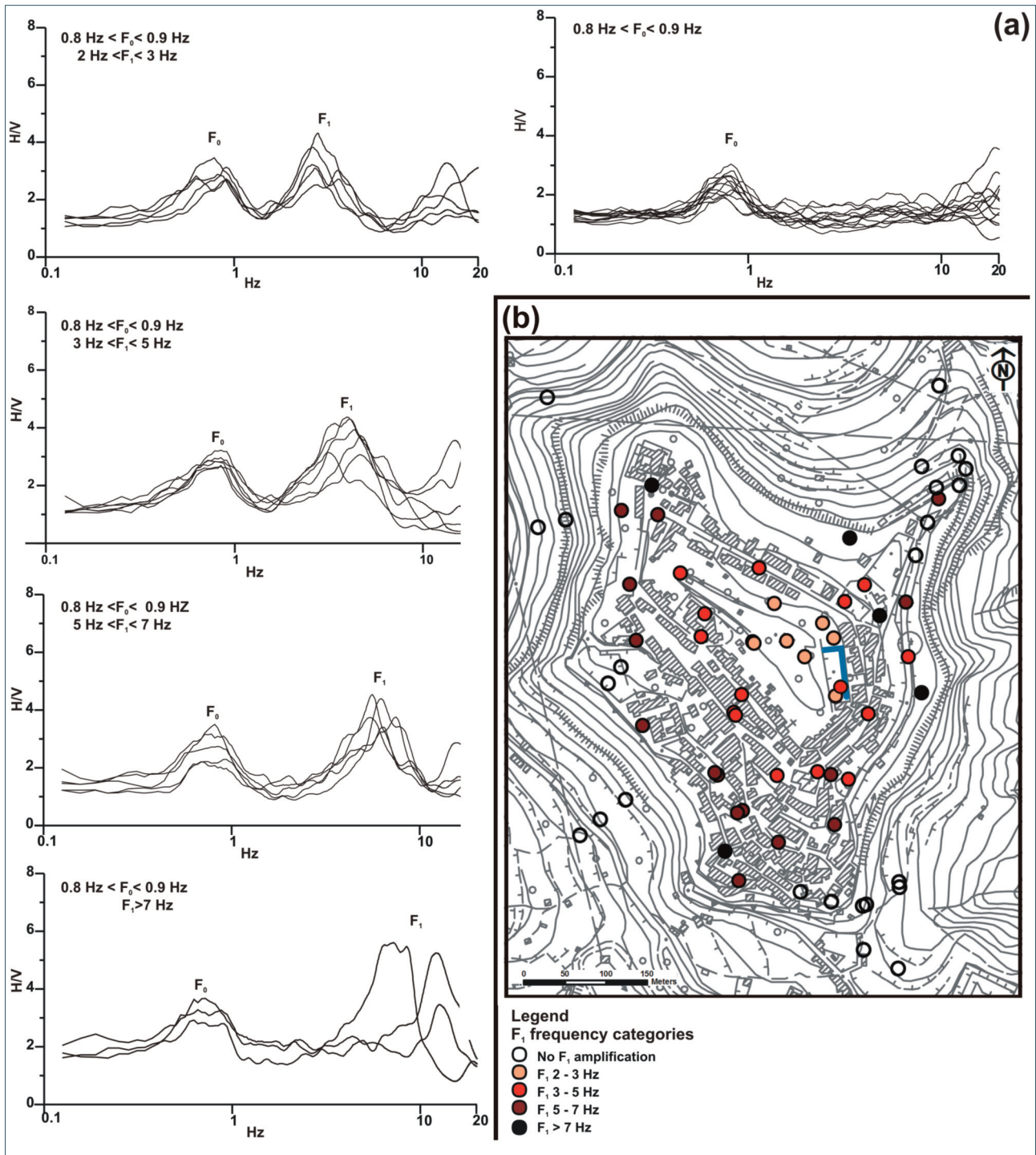


FIGURE 3. (a) Examples of H/V curves classified according to the F_1 frequency categories. (b) Topographic map of Rometta showing: location of the 64 single-station H/V measurement points sampled by the F_1 frequency categories (see legend for details), and the array configuration (blue line).

2002; Okada, 2003].

Several single-station recordings were also taken close to the array, to determine whether the sampled area beneath the array consists of approximately homogeneous strata. If the resulting H/V curves, as in this case (Figure 4), had the same peak frequency this was taken as an indication that the sediment cover

was uniform over the array area, satisfying one of the key assumptions of the array methods [Parolai et al., 2001; 2004; Farrugia et al., 2016, 2017]. Finally, the one-dimensional V_S profiles were obtained by inverting both H/V and effective dispersion curves in a joint inversion procedure based on the Genetic Algorithm [GA; Yamanaka and Ishida, 1996; Picozzi and

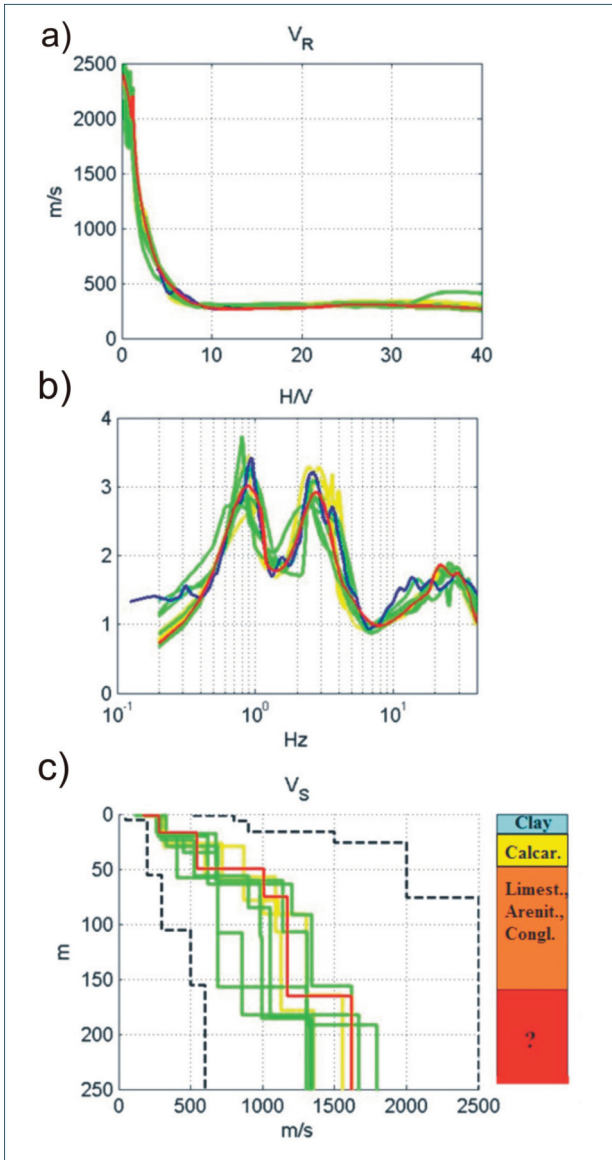


FIGURE 4. The figure reports the joint inversion results and relative stratigraphic interpretation. (a) Comparison among the experimental dispersion curve (blue line) and the theoretical ones (red line is the best fitting theoretical curve; green and yellow lines are the curves characterized by a misfit that is within 50% and greater than 150% of the best model’s misfit value, respectively). (b) Comparison among the experimental H/V curve (blue line) and the theoretical ones (red line is the best fitting theoretical curve; green and yellow lines are the curves characterized by a misfit that is within 50% and greater than 150% of the best model’s misfit value, respectively). (c) The V_S best profiles from each of the 10 inversions carried out. Dashed black lines represent the limits of the GA search. The stratigraphic interpretation is shown on the right.

Albarello, 2007; Parolai et al., 2005; Arai and Tokimatsu, 2005]. The advantage of the joint inversion procedure is that it utilizes the two data sets, which are sensitive to different properties. Scherbaum et al. [2003] showed that while the dispersion curve con-

strains the V_S of the sedimentary cover, the H/V peak frequency constrains the thickness H . The GA is an iterative procedure that focuses exploration in the more promising areas within a research space [Albarello et al., 2011]. From the initial 100 randomly generated models, a number of best models are selected and genetic operators (cross-over, mutation and elite selection) are applied to simulate genetic selection and create a second generation of models. The processes were repeated through 150 iterations. Ten separate inversions were run and the best-fitting profile for each inversion was saved.

The final result was chosen as the one characterized by the minimum misfit value (i.e. whose synthetic H/V and effective dispersion curves best fit the experimental ones, in accordance with the established measures) from all 10 inversions. The other best results are useful to estimate the inversion result variability and robustness. In each inversion the number of layers of variable thickness was kept fixed (to match the known outcropping geological sequence) while the shear wave velocity in each layer was allowed to vary over a wide range of values, with no a priori assumption [Picozzi and Albarello, 2007]. Theoretical HVSR and effective dispersion curves were computed assuming the subsoil as a flat stratified viscoelastic medium where only surface waves (Rayleigh and Love) propagate [Lunedei and Albarello, 2009]. Higher propagation modes were considered and the unique “effective” dispersion curve (Rayleigh-wave phase velocity vs. frequency) was used. In presence of higher mode Rayleigh waves, the curve would contain contributions from higher modes of propagation that cannot be resolved due to limited resolution of the finite array [Foti et al., 2015]. The use of the effective dispersion curve avoids the picking of the different propagation modes that can be problematic [Albarello et al., 2011]. It is well known that higher modes can dominate certain frequency ranges [e.g. Tokimatsu, 1997; Zhang and Lu, 2003; Arai and Tokimatsu, 2004]. Higher modes are more sensitive to deeper structure than the fundamental one and thus their inclusion in the inversion stabilizes the process and increases the resolution of the inverted profiles augmenting the resolvable depth of the profile. The procedure gives reliable results, usually closer to the available V_S data, deriving from geophysical surface seismic method (MASW) made for civil engineering purposes, than the ones obtained using conventional inversion procedures [e.g., Picozzi et al., 2009; Panzera and Lombardo, 2013; Panzera et al., 2012, 2013; Shabani et al., 2008].

4. RESULTS AND DISCUSSION

The H/V results from the data set collected in Rometta show significant peaks at frequencies ranging approximately from 0.5 Hz to 15 Hz (Figure 3, see also the supplementary material). Most of the investigated sites show two-peak curves indicating a subsoil locally characterized by two significant impedance contrasts at different depths. A fundamental resonance frequency F_0 ranging from 0.5 Hz to 0.9 Hz can be observed at all measurement sites and a secondary peak F_1 generally lies in the 2.5 - 15 Hz interval. In the whole study area the F_0 peak can be related to a seismic reflector referable to metamorphic bedrock that we may locate at a depth greater than 100 m beneath each individual measurement site according to Albarello and Castellaro [2011]. Geological analysis indicates a bedrock depth of the order of 200 m beneath the top of the Rometta hill (see Figure 2b). The F_1 peaks suggest a shallow seismic interface with variable depth, which on the basis of seismic velocities estimated by array analyses (see later) can be imputed to clay-calcareous transition. It is noteworthy that such a transition, and therefore the presence of the clay, is detected almost everywhere in the Rometta hill, in particular even where the geological maps [Lentini et al., 2000; APAT, 2008, Figure 2c, d] indicate Upper-Pliocene-Lower-Pleistocene calcarenites outcrops.

The H/V method is widely used for site investigations due to its capability of estimating the fundamental resonance frequency of a site, F_0 , which is related to the travel-time average shear-wave velocity $\langle V_s \rangle$ of a surface sedimentary cover with thickness H above the bedrock by,

$$F_0 = \frac{\langle V_s \rangle}{4H} \quad (1)$$

The results of the joint inversion of phase velocity dispersion and H/V ratio curves for obtaining local S-wave velocity profile from seismic noise recordings are shown in Figure 4. A good match between the theoretical and experimental dispersion curves and H/V peak can be observed (Figure 4a, b). Then we used the derived shear-wave velocity for the clay formation obtained by the joint inversion to model and interpreted all H/V curves. The first layer of the model with the least misfit has a thickness of ca. 20 m and V_s of 250-500 m/s and it is compatible with soft clay lithologies. This implies that the study area presents an impedance contrast related to the clays-calcareous interface in agreement with the resonance frequencies F_1 estimated. The values of F_1 (2.5 - 15 Hz) increase from the top of the central sector of the Rometta urban area up to the edge

of surrounding cliffs where F_1 disappear (Figure 3), indicating a progressive reduction of the thickness of the clay. Therefore, our analyses reveal that the Middle-Pleistocene blue marly clays have a greater extension with respect to the available geological data [Lentini et al., 2000; APAT, 2008], thus reversing the erroneous belief that most of Rometta village is located on calcarenitic rocks (Figure 5).

We may note some correspondence between the wider Middle-Pleistocene blue marly clays distribution observed in the present study and the past earthquake damage distribution [Baratta, 1910], thus indicating the local geology as possible responsible of amplification effects. In fact, collapses and dramatic failures occurred in those sectors where the clays overcrop while is testified the resilience of the VI century Church of SS. Salvatore, located where the calcarenitic unit outcrops (Figure 5). Moreover, the H/V results collected in Rometta do not seem to be significantly influenced by topographic effects. The ubiquitous fundamental resonance frequency F_0 peaks (0.5-0.9 Hz) indicate that the sedimentary sequence-bedrock contrast is detectable both on hilltop and in close proximity of the cliff face. Finally, this result was obtained by using passive seismic techniques particularly useful in those areas as Rometta where surface geology is obscured by urbanization and intense vegetation cover.

5. CONCLUDING REMARKS

Passive seismic surface-wave measurements have been used to obtain one-dimensional shear-wave velocity profiles and physical characterization of the different lithologies in the Rometta area. The H/V technique revealed a ubiquitous fundamental frequency (F_0) between 0.5 Hz and 0.9 Hz and secondary frequency peaks (F_1) from 2.5 Hz to 15 Hz. The fundamental frequency (F_0) is ascribed to the interface with the metamorphic bedrock with a depth of about 200 m. The (F_1) frequency range is associated with the variable thickness of the clay layer that decrease moving from the center of the top hill towards the edge of the cliff (Figure 5). These results suggest a wider extension of the outcropping clays with respect to previously available knowledge, that could be responsible for the past earthquake damage distribution observed. This can have some important implications for microzonation analysis and seismic risk assessment because the most accurate geological knowledge of the area enables a correct seismic soil classification. Furthermore, this study justifies the use of the ESAC method, the joint inversion

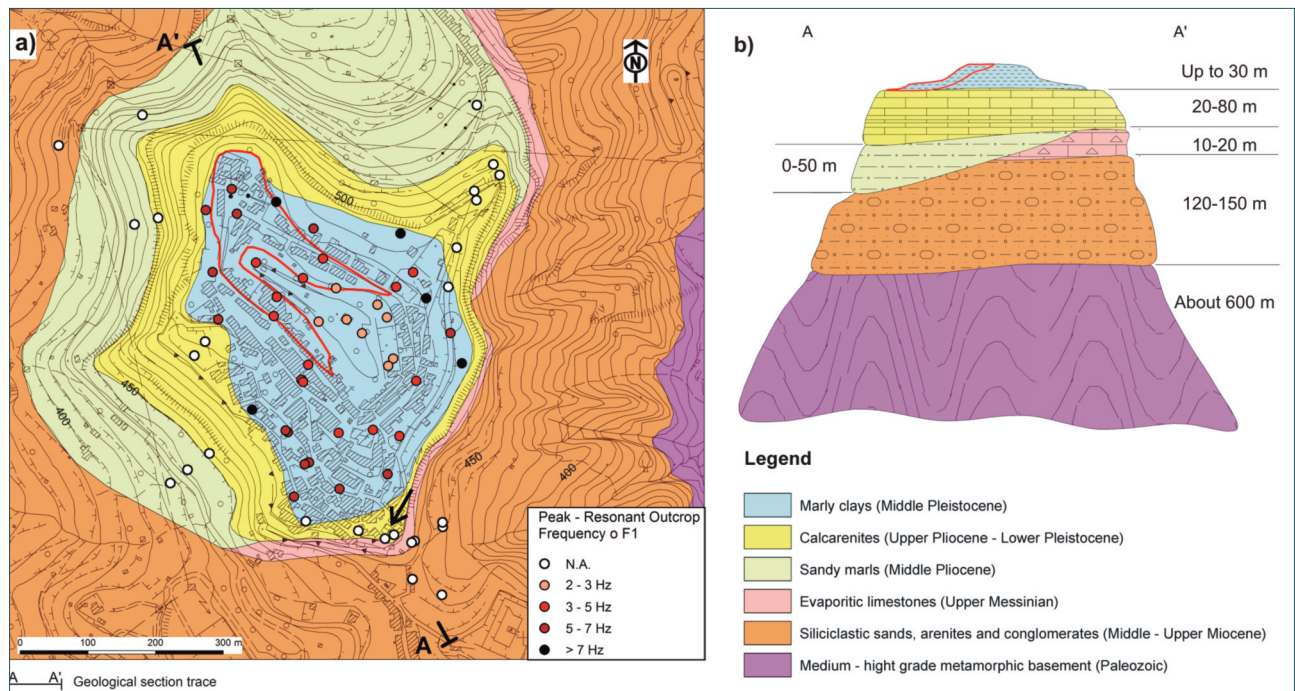


FIGURE 5. (a) New geological sketch map of Rometta that compares the clay extension (see legend) based on our geophysical results. For comparison is also show the clay extension (red line) by the most recent geological map [APAT, 2008]. The black arrow indicates the building of the VI century Church of SS. Salvatore, undamaged by the 1908 earthquake [Baratta, 1910]. (b) Stratigraphic framework from A to A' of the Rometta succession.

and genetic inversion algorithm, which have been shown to be effective in resolving the velocity profile in the stratigraphy of the study area. Based on the interpretation of geophysical results a new geological map is also proposed, which includes a wider extension of the clays with respect to previously available geological maps (Figure 5). We emphasize that accurate geological field surveys combined with geophysical analysis can contribute to extend geological knowledge and better define geological models for seismic hazard and risk assessment studies. The geophysical methods used should be applied for mapping surface geology in many other urban areas in Italy where geology is obscured and data interpretation is difficult.

The results of the present study represent an important step towards a holistic seismic risk assessment in the area and they will serve as an input to the mapping of ground motion scenarios. They will shed light on possible amplification effects helping to better understand the pattern and damage distribution of historical earthquakes.

Acknowledgements. The authors thank Editor Mario Mattia and two anonymous reviewers for useful comments and suggestions, which allowed us to improve the article. This research has benefited from funding provided by PO-FESR 2007/2013 Project 'Attività di sviluppo sperimentale finalizzata alla riduzione del rischio sismico nella Sicilia Orientale'.

DATA AND SHARING RESOURCES

<https://emidius.mi.ingv.it/CPT115-DBMI15/>

REFERENCES

- Albarelo, D., Cesi, C., Eulilli, V., Guerrini, F., Lunedei, E., Paolucci, E., Pileggi, D., Puzzilli, L. M. (2011). The contribution of the ambient vibration prospecting in seismic microzoning: an example from the area damaged by the April 6, 2009 L'Aquila (Italy) earthquake. *Boll. Geof. Teor. Appl.*, 52, 513-538.
- Albarelo, D., and Castellaro, S. (2011). Tecniche sismiche passive: indagini a stazione singola, *Ing. Sism.*, 38(2), 32-49.
- APAT (2008). *Carta Geologica d'Italia alla scala 1: 50.000, Foglio 601 Messina-Reggio di Calabria*, S. EL. CA, Firenze.
- Arai, H., and Tokimatsu, K. (2004). S-wave velocity profiling by inversion of microtremor H/V spectrum. *Bulletin of the Seismological Society of America*, 94(1), 53-63.
- Arai, H., and Tokimatsu, K. (2005). S-wave velocity profiling by joint inversion of microtremor dispersion curve and horizontal-to-vertical (H/V) spectrum, *Bull. Seism. Soc. Am.*, 95(5), 1766-1778.
- Baratta, M. (1910). La catastrofe sismica Calabro messinese (28 dicembre 1908). *Società geografica italiana*.

- Bard, P. Y. (1999). Microtremor measurements: a tool for site effect estimation. The effects of surface geology on seismic motion, 3, 1251-1279.
- Bard, P. Y. (2005). Guidelines for the implementation of the H/V spectral ratio technique on ambient vibrations: measurements, processing, and interpretations. SESAME European research project. WP12, deliverable D23.12, 2004.
- Bonini, L., Di Bucci, D., Toscani, G., Seno, S., Valensise, G. (2011). Reconciling deep seismogenic and shallow active faults through analogue modeling: the case of the Messina Straits (southern Italy), *J. Geol. Soc. Lond.* 168: 191-199.
- Bonnefoy-Claudet, S., Cotton, F., and Bard, P. Y. (2006a). The nature of noise wavefield and its applications for site effects studies: a literature review; *Earth-Science Reviews*, 79(3), 205-227.
- Bonnefoy-Claudet, S., Cornou, C., Bard, P. Y., Cotton, F., Moczo, P., Kristek, J., Fäh, D. (2006b). H/V ratio: a tool for site effects evaluation. Results from 1-D noise simulations, *Geophys. J. Int.*, 167(2), 827-837.
- Calais, E., Nocquet, J. M., Jouanne, F. and Tardy, M. (2002). Current strain regime in the Western Alps from continuous Global Positioning System measurements, 1996-2001. *Geology*, 30(7), 651-654.
- Cara, F., Di Giulio, G., Rovelli, A. (2003). A study on seismic noise variations at Colfiorito, central Italy: implications for the use of H/V spectral ratios, *Geophys. Res. Lett.* 30, no. 18, 1972, doi 10.1029/2003GL017807.
- Castellaro, S., and Mulargia, F. (2009). The effect of velocity inversions on H/V, *Pure Appl. Geophys.*, 166(4), 567-592.
- D'Amico, V., Picozzi M., Baliva F., Albarello D. (2008). Ambient noise measurements for preliminary site-effects characterization in the urban area of Florence, Italy, *Bull. Seism. Soc. Am.*, 98.3, 1373-1388.
- Di Stefano, A., Longhitano, S., Smedile, A. (2007). Sedimentation and tectonics in a steep shallow-marine depositional system: stratigraphic arrangement of the Pliocene-Pleistocene Rometta Succession (NE Sicily, Italy), *Geol. Carpath.*, 58(1), 71.
- Faccenna, C., Becker T. W., Lucente F. P., Jolivet L. (2001). History of subduction and back arc extension in the Central Mediterranean, *Geophys. J. Int.*, 145.3, 809-820.
- Fäh D., Kind F., Giardini D. (2001). A theoretical investigation of average H/V ratios, *Geophys. J. Int.*, 145, 535-549.
- Farrugia, F., Paolucci, E., D'Amico, S., Galea, P. (2016). Inversion of surface-wave data for subsurface shear-wave velocity profiles characterised by a thick buried low-velocity layer. *Geophysical Journal International*, 206, 1221-1231, doi:10.1093/gji/ggw204
- Farrugia, D., Galea, P., D'Amico, S., Paolucci, E. (2017). Sensitivity of ground motion parameters to local shear-wave velocity models: The case of buried low-velocity layers. *Soil Dynamics and Earthquake Engineering*, 100, 196-205, <http://dx.doi.org/10.1016/j.soildyn.2017.05.033>
- Foti, S., Lai, C.G., Rix, G.J. and Strobbia C. (2015). *Surface Wave Methods for Near-Surface Site Characterization*. Florida: CRC Press.
- Ghisetti, F., and Vezzani, L. (1982). Strutture tensionali e compressive indotte da meccanismi profondi lungo la linea del Pollino (Appennino meridionale), *Boll. Soc. Geol. Ital.*, 101(3), 385-440.
- Guarnieri, P., and Carbone, S. (2003). Assetto geologico e lineamenti morfostutturali dei bacini plio-quaternari del Tirreno meridionale, *Boll. Soc. Geol. Ital.*, 122(3), 377-386.
- Gueguen, E., Doglioni C., Fernandez M. (1997). Lithospheric boudinage in the Western Mediterranean back-arc basin, *Terra Nova*, 9.4 184-187.
- Konno, K., and Ohmachi, T. (1998). Ground-motion characteristics estimated from spectral ratio between horizontal and vertical components of microtremor. *Bull. Seism. Soc. Am.*, 88(1), 228-241.
- Lachet, C. and Bard, P. Y. (1994). Numerical and Theoretical Investigations on the Possibilities and Limitations of Nakamura's Technique, *J. Phys. Earth*, 42(5), 377-397.
- Lentini, F., Carbone, S., Catalano, S., Messina (Provincia). Assessorato territorio. Servizio geologico. (2000). Carta geologica della provincia di Messina, S. EL. CA.
- Lermo, J., and Chávez-García, F. J. (1993). Site effect evaluation using spectral ratios with only one station, *Bull. Seism. Soc. Am.*, 83(5), 1574-1594.
- Locati, M., Camassi, R., Rovida, A., Ercolani, E., Bernardini, F., Castelli, V., Caracciolo, C.H., Tertulliani, A., Rossi, A., Azzaro, R., D'Amico, S., Conte, S., Rocchetti, E. (2016). DBMI15, the 2015 version of the Italian Macroseismic Database. Istituto Nazionale di Geofisica e Vulcanologia. doi:<http://doi.org/10.6092/INGV.IT-DBMI15>.
- Lunedei, E., & Albarello, D. (2009). On the seismic noise wavefield in a weakly dissipative layered Earth. *Geophysical Journal International*, 177(3), 1001-1014.
- Malinverno, A., and Ryan, W. B. (1986). Extension in the Tyrrhenian Sea and shortening in the Apennines as result of arc migration driven by sinking of the lithosphere, *Tectonics*, 5(2), 227-245.
- Malischewky P.G. and Scherbaum F. (2004). Love's formula and H/V ratio (ellipticity) of Rayleigh waves, *Wave Motion*, 40, 57-67.

- Montenat, C., Barrier, P., d'Estevou, P. O. (1991). Some aspects of the recent tectonics in the Strait of Messina, Italy, *Tectonophysics*, 194(3), 203-215.
- Nakamura, Y. (1989). A method for dynamic characteristics estimation of subsurface using microtremor on the ground surface, *Quarterly Report Railway Tech. Res. Inst.*, 30(1), 25-30.
- Nakamura, Y. (1996). Real-time information systems for hazards mitigation, *Proceedings of the 11th World Conference on Earthquake Engineering*, Acapulco, Mexico.
- Nocquet, J. M. and Calais, E. (2004). Geodetic measurements of crustal deformation in the Western Mediterranean and Europe. In *Geodynamics of Azores-Tunisia* (pp. 661-681). Birkhäuser Basel.
- Nocquet, J. M. (2012). Present-day kinematics of the Mediterranean: A comprehensive overview of GPS results. *Tectonophysics*, 579, 220-242.
- Nogoshi, M. and T. Igarashi (1971). On the amplitude characteristics of microtremor (part 2), *J. Seismol. Soc. Japan*, 24, 26-40.
- Ohori, M., Nobata, A., Wakamatsu, K. (2002). A comparison of ESAC and FK methods of estimating phase velocity using arbitrarily shaped microtremor arrays, *Bull. Seism. Soc. Am.*, 92(6), 2323-2332.
- Okada, H. 2003. The microtremor survey method. *Geophysical Monograph Series*, Society of Exploration Geophysicists 12.
- Panzerà, F., D'Amico, S., Lotteri, A., Galea, P., Lombardo G. (2012). Seismic site response of unstable steep slope using noise measurements: the case study of Xemxija bay area, Malta. *Nat. Hazards Earth Syst. Sci.*, 12, 3421-3431, doi:10.5194/nhess-12-3421-2012.
- Panzerà, F., D'Amico, S., Galea, P., Lombardo, G., Gallipoli, M. R., Pace, S. (2013). Geophysical measurements for site response investigation: preliminary results on the island of Malta, *Boll. Geof. Teor. Appl.*, 54(2), 111-128.
- Panzerà, F. and G. Lombardo (2013). Seismic property characterization of lithotypes cropping out in the Siracusa urban area, Italy. *Eng. Geol.*, 153, 12-24.
- Paolucci E., Albarello D., D'Amico S., Lunedei E., Martelli L., Mucciarelli M., Pileggi D., (2015). A large scale ambient vibration survey in the area damaged by May-June 2012 seismic sequence in Emilia Romagna, Italy. *Bulletin of Earthquake Engineering*, doi:10.1007/s10518-015-9767-5
- Parolai, S., Bormann, P., Milkereit, C. (2001). Assessment of the natural frequency of the sedimentary cover in the Cologne area (Germany) using noise measurements, *J. Earthq. Engrg.*, 5, 541-564.
- Parolai, S., Richwalski, S., M., Milkereit, C., Bormann, P. (2004). Assessment of the stability of H/V spectral ratio from ambient noise and comparison with earthquake data in the Cologne area (Germany), *Tectonophysics*, 390, 57-73.
- Parolai, S., Picozzi, M., Richwalski, S. M., Milkereit, C. (2005). Joint inversion of phase velocity dispersion and H/V ratio curves from seismic noise recordings using a genetic algorithm, considering higher modes, *Geophys. Res. Lett.*, 32(1).
- Parolai, S., Richwalski, S. M., Milkereit, C., Fäh, D. (2006). S-wave velocity profiles for earthquake engineering purposes for the Cologne area (Germany), *Bull. Earthq. Eng.*, 4 (1), 65-94.
- Picozzi, M., and Albarello, D. (2007). Combining genetic and linearized algorithms for a two-step joint inversion of Rayleigh wave dispersion and H/V spectral ratio curves, *Geophys J. Int.*, 169(1), 189-200.
- Picozzi, M., Parolai, S., Bindi, D., Strollo, A. (2009). Characterization of shallow geology by high-frequency seismic noise tomography, *Geophys J. Int.*, 176(1), 164-174.
- Scherbaum, F., Hinzen, K.G., Ohrnberger, M. (2003). Determination of shallow shear wave velocity profiles in the Cologne, Germany area using ambient vibrations, *Geophys J. Int.*, 152, 597-612.
- Scolaro, S., Pino, P., D'Amico, S., Orecchio, B., Presti, D., Torre, A., Totaro, C., Farrugia, D., Neri, G. (2018). Ambient noise measurements for preliminary microzoning studies in the city of Messina, Sicily, accepted for publication in *Annals of Geophysics*, Special Number on "Seismic Risk Reduction in Eastern Sicily".
- Shabani, E., Cornou, C., Hagshenas, M., Wathelet, M., Bard, P. Y., Mirzaei, N., Eskandari-Ghadi, M. (2008). Estimating shear-waves velocity structure by using array methods (FK and SPAC) and inversion of ellipticity curves at a site in south of Tehran, 14th Word Conference on Earthquake Engineering, pp. 12-17.
- Tokimatsu, K. (1997). Geotechnical site characterization using surface waves. In *Proc. 1st Inter. Conf. on Earthquake Geotechnical Engineering*, Tokyo, 1997 (Vol. 3, pp. 1333-1368).
- Tortorici, L., Monaco, C., Tansi, C., Cocina, O. (1995). Recent and active tectonics in the Calabrian arc (Southern Italy), *Tectonophysics*, 243(1), 37-55.
- Vella, A., Galea, P., D'Amico, S. (2013). Site response characterisation of the Maltese islands based on ambient noise HVSR, *Engineering Geology*, 163, 89-100. doi:10.1016/j.enggeo.2013.06.006.
- Violanti, D. (1989). Foraminiferi plio-pleistocenici del ver-

sante settentrionale dei monti Peloritani: analisi biostratigrafica e paleoambientale, Riv. Ital. Paleontol. S., 95(2), 173-216.

Westaway, R. (1993). Quaternary uplift of southern Italy, J. Geophys. Res.-Sol. Ea., 98(B12), 21741-21772.

Yamanaka, H. and Ishida, H. (1996). Application of genetic algorithms to an inversion of surface-wave dispersion data, Bull. Seism. Soc. Am., 86(2), 436-444.

Zhang, B., and Lu, L. (2003). Rayleigh wave and detection of low-velocity layers in a stratified half-space. Acoustical Physics, 49(5), 516-528.

***CORRESPONDING AUTHOR:** Silvia SCOLARO,

Department of Mathematics, Computer Sciences, Physics and Earth Sciences
University of Messina, Messina, Italy
email: silscolaro@unime.it

© 2018 the Istituto Nazionale di Geofisica e Vulcanologia.

All rights reserved.

Supplemental Material for

**INTEGRATION OF GEOLOGICAL AND GEOPHYSICAL
DATA FOR RE-EVALUATION OF LOCAL SEISMIC
HAZARD AND GEOLOGICAL STRUCTURE:
THE CASE STUDY OF ROMETTA, SICILY (ITALY)**

Paolo Pino¹, Sebastiano D'Amico², Barbara Orecchio¹, Debora Presti¹,
Silvia Scolaro¹, Antonino Torre¹, Cristina Totaro¹, Daniela Farrugia², Giancarlo Neri¹

¹Department of Mathematics, Computer Sciences, Physics, and Earth Sciences, University
of Messina, Messina, Italy

²Department of Geosciences, University of Malta, Malta

INTRODUCTION

The auxiliary material includes sixty-five plots (see Figures S1-S2).
These provide the complete set of HVSR curves obtained in the
present study.

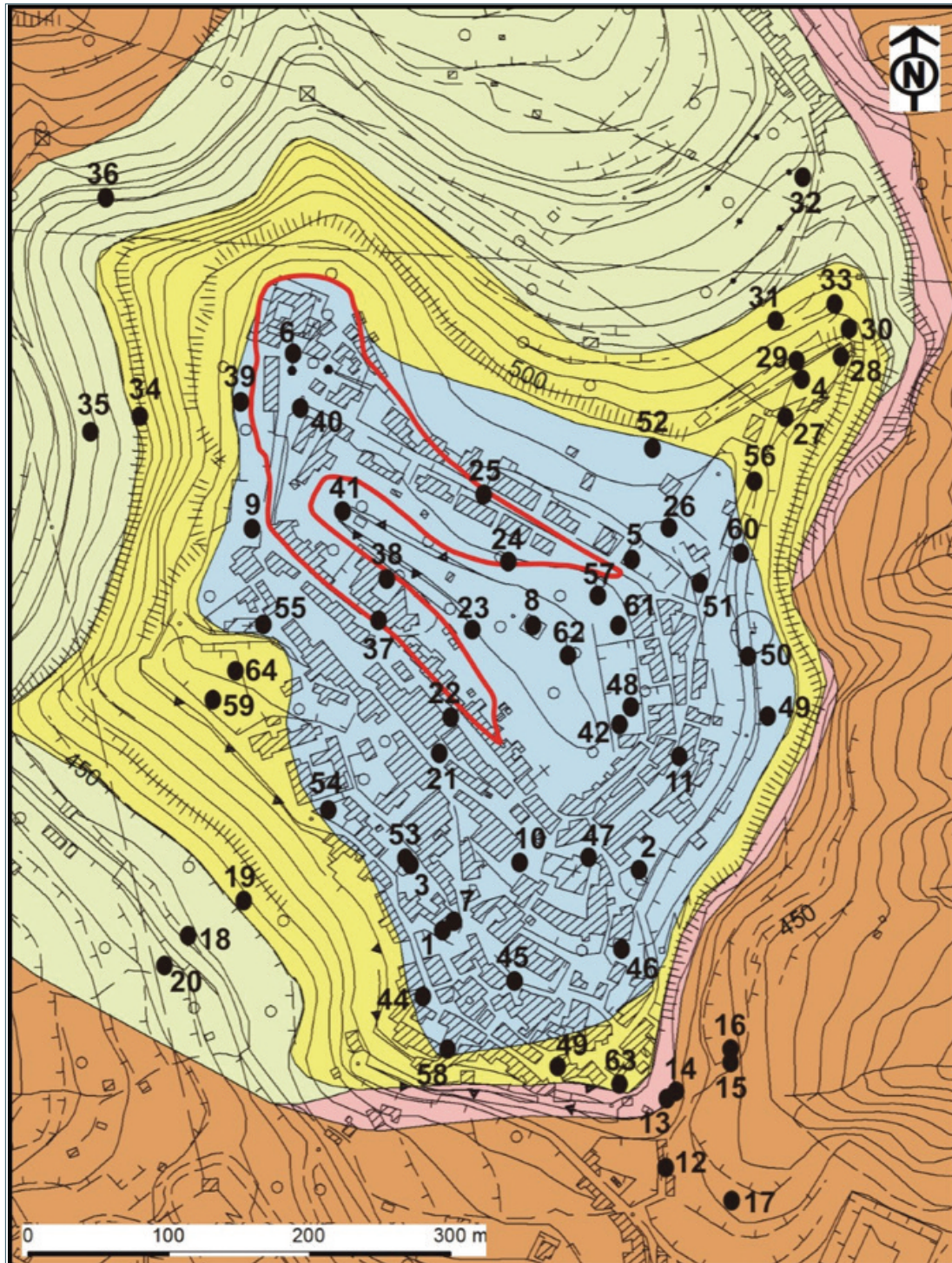


FIGURE S1. HVSR measurement points superimposed on the geological map of Rometta proposed in the present study.

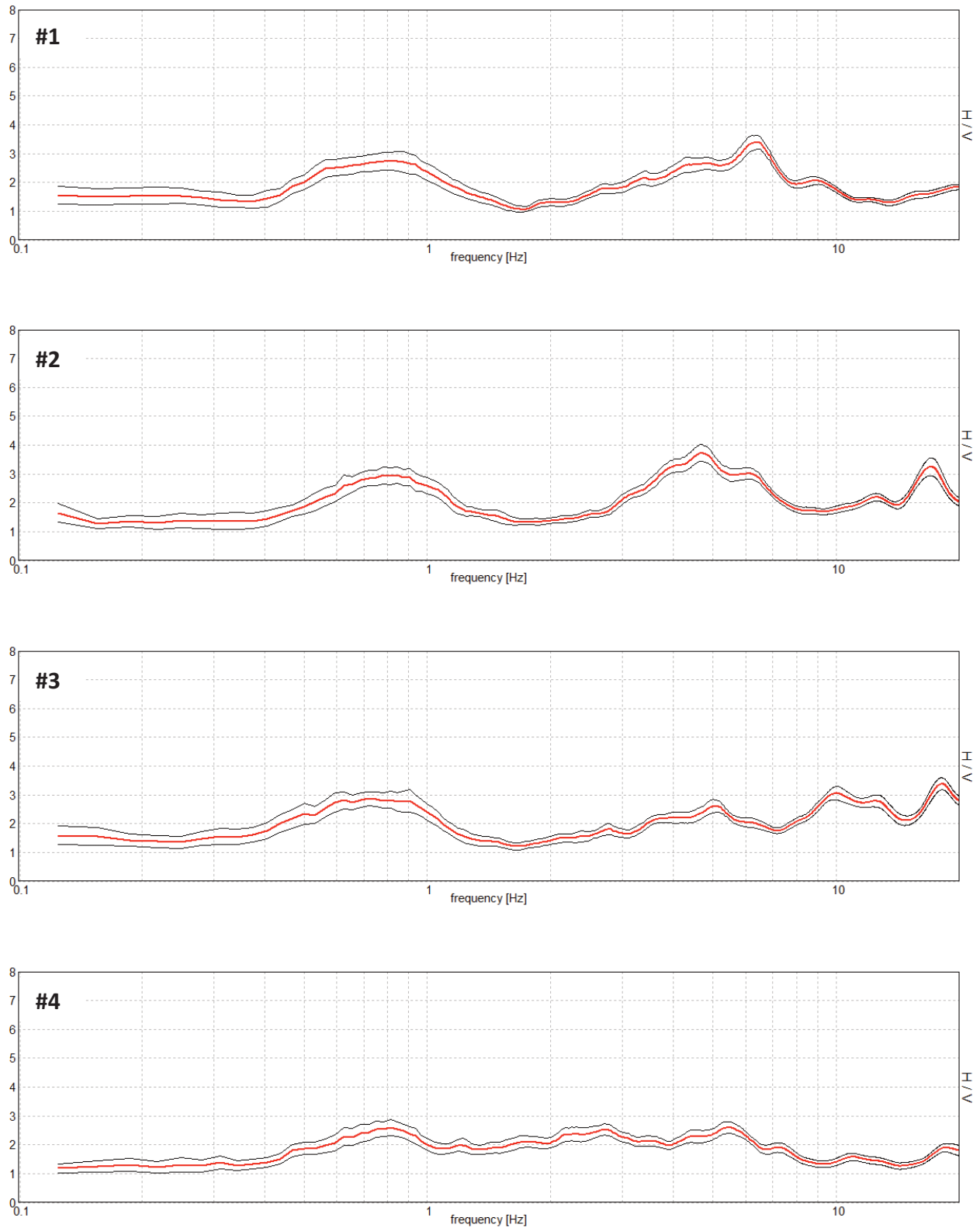


FIGURE S2. HVSR curves relative to the measurement points shown in Figure S1 (#64). Red curve = mean spectral ratio, black curves = standard deviation.

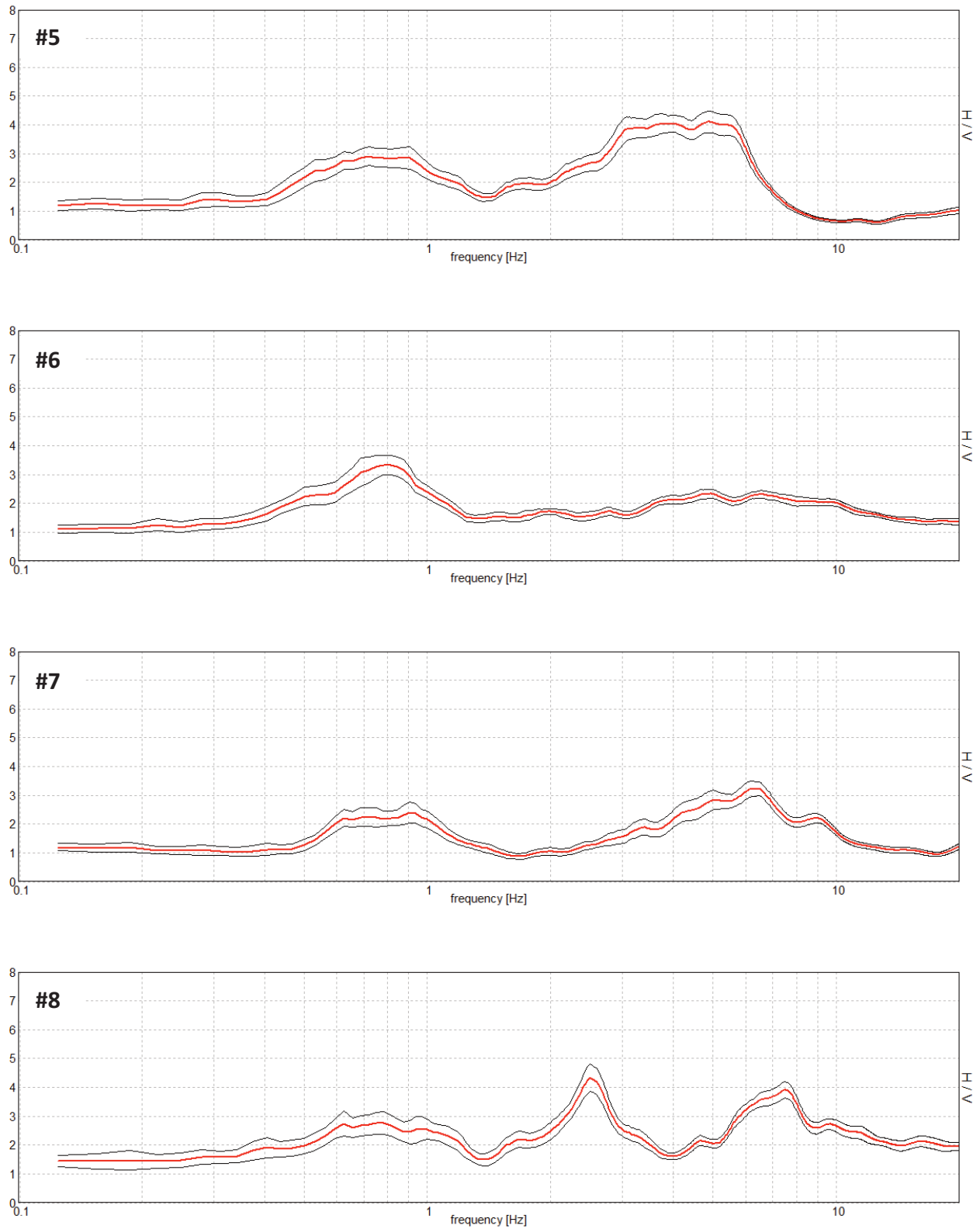


FIGURE S2. HVSR curves relative to the measurement points shown in Figure S1 (#64). Red curve = mean spectral ratio, black curves = standard deviation.

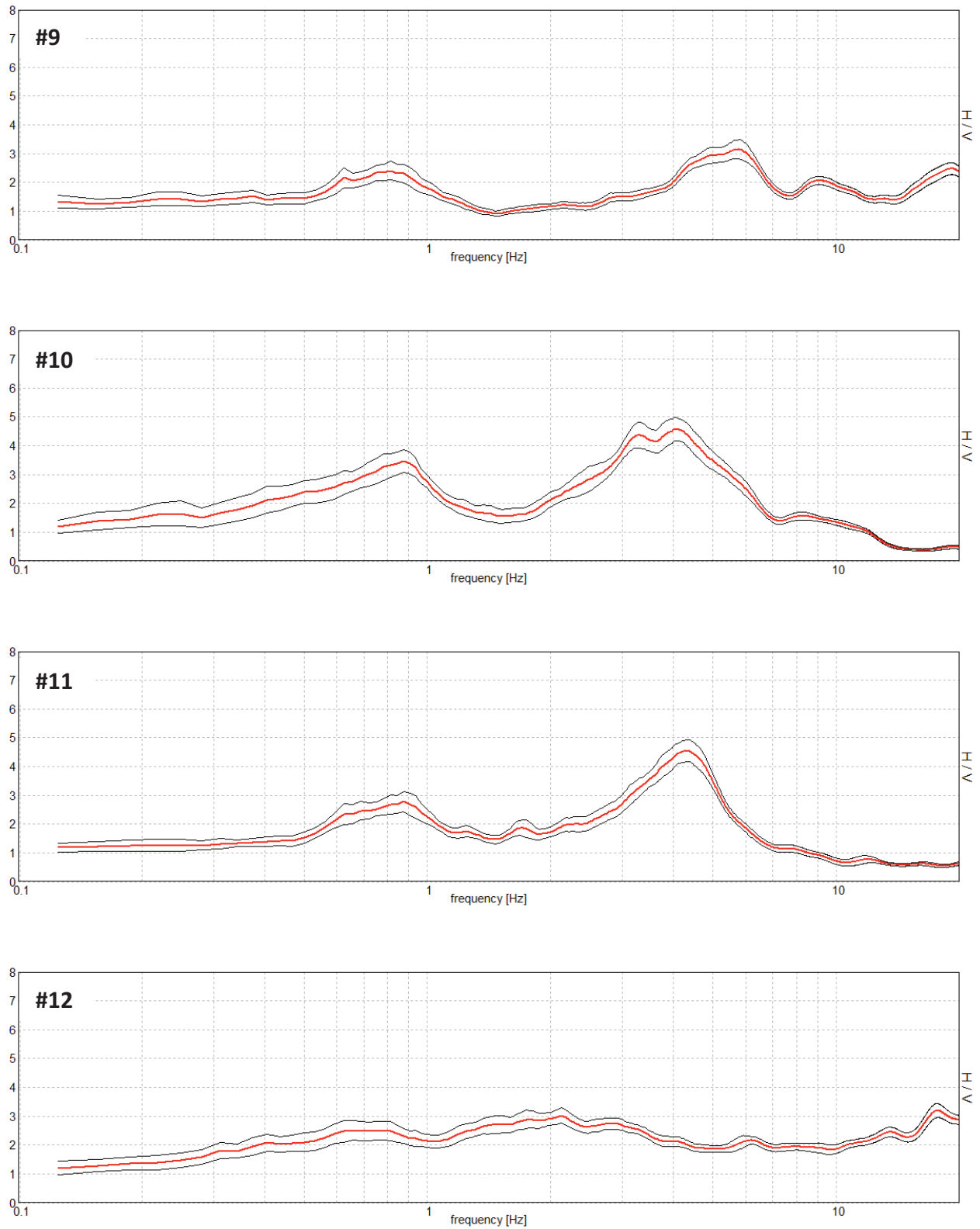


FIGURE S2. HVSR curves relative to the measurement points shown in Figure S1 (#64). Red curve = mean spectral ratio, black curves = standard deviation.

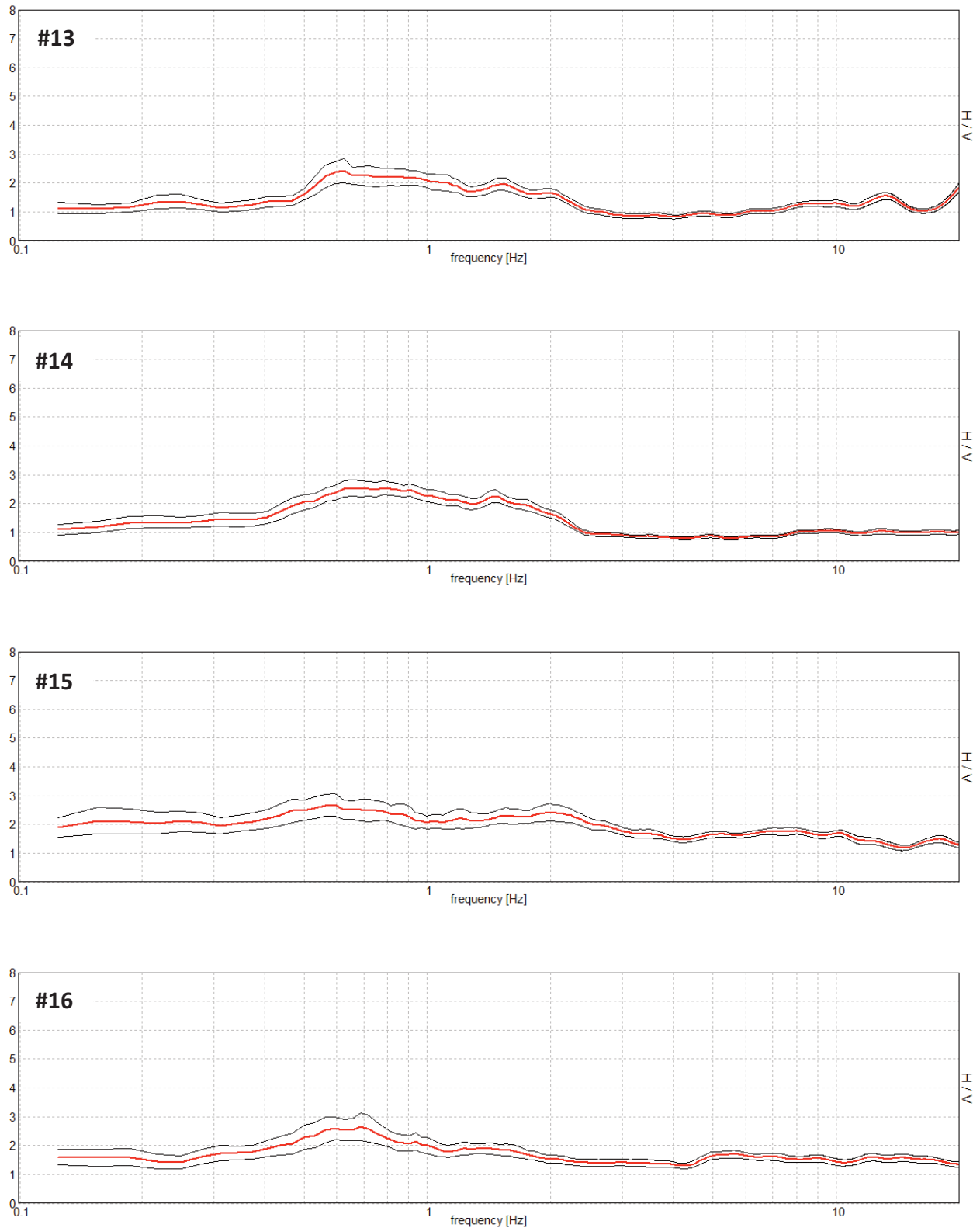


FIGURE S2. HVSR curves relative to the measurement points shown in Figure S1 (#64). Red curve = mean spectral ratio, black curves = standard deviation.

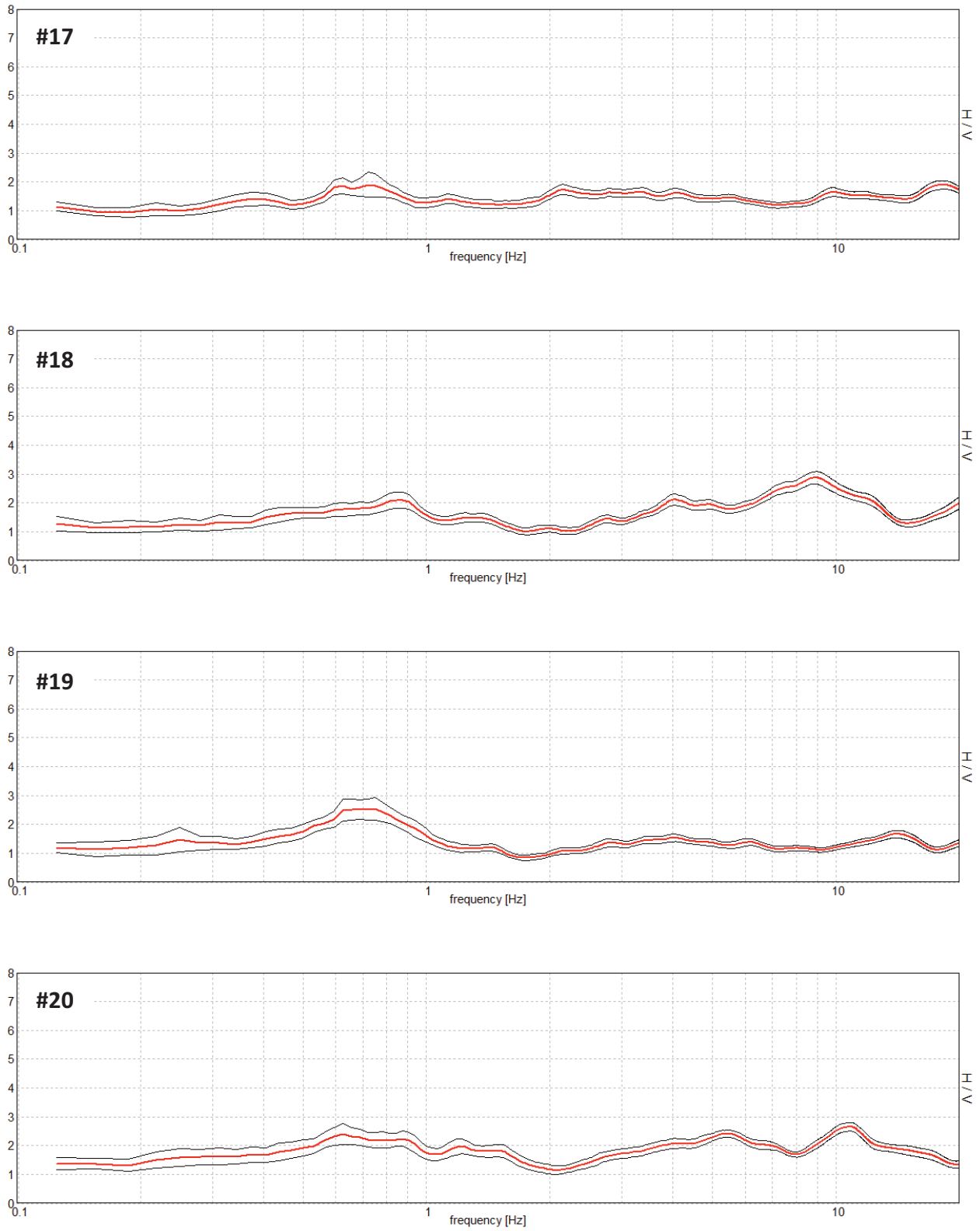


FIGURE S2. HVSR curves relative to the measurement points shown in Figure S1 (#64). Red curve = mean spectral ratio, black curves = standard deviation.

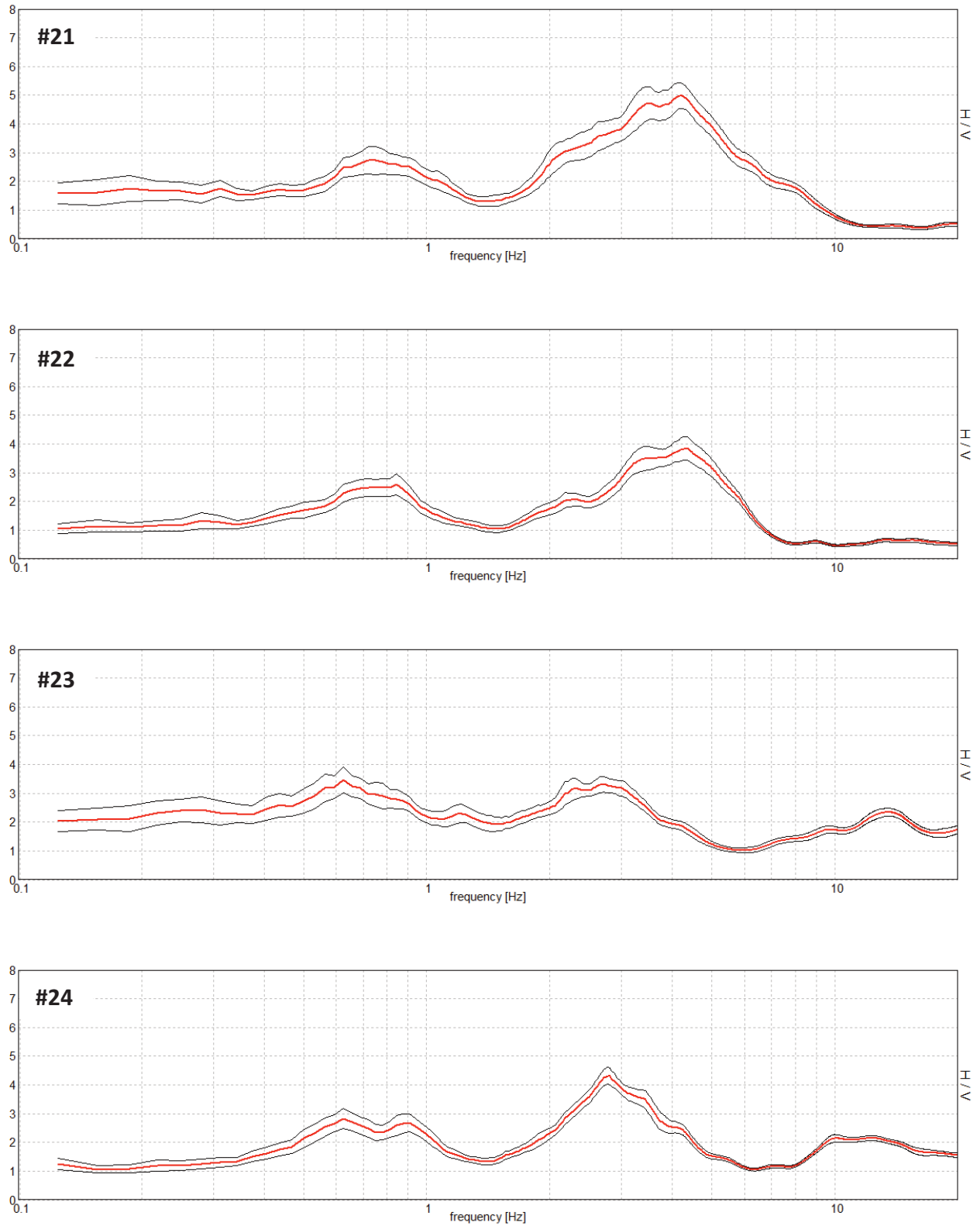


FIGURE S2. HVSR curves relative to the measurement points shown in Figure S1 (#64). Red curve = mean spectral ratio, black curves = standard deviation.

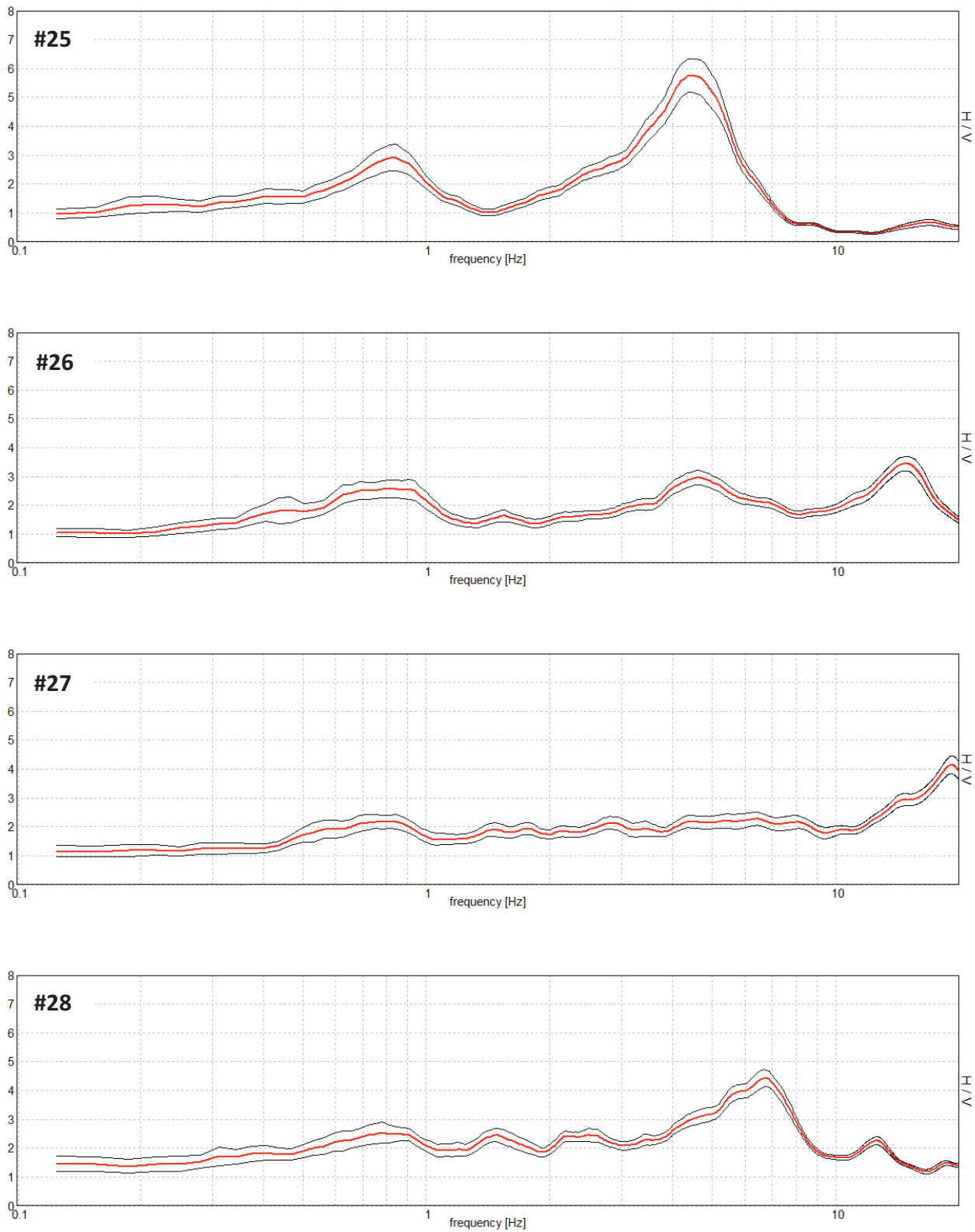


FIGURE S2. HVSR curves relative to the measurement points shown in Figure S1 (#64). Red curve = mean spectral ratio, black curves = standard deviation.

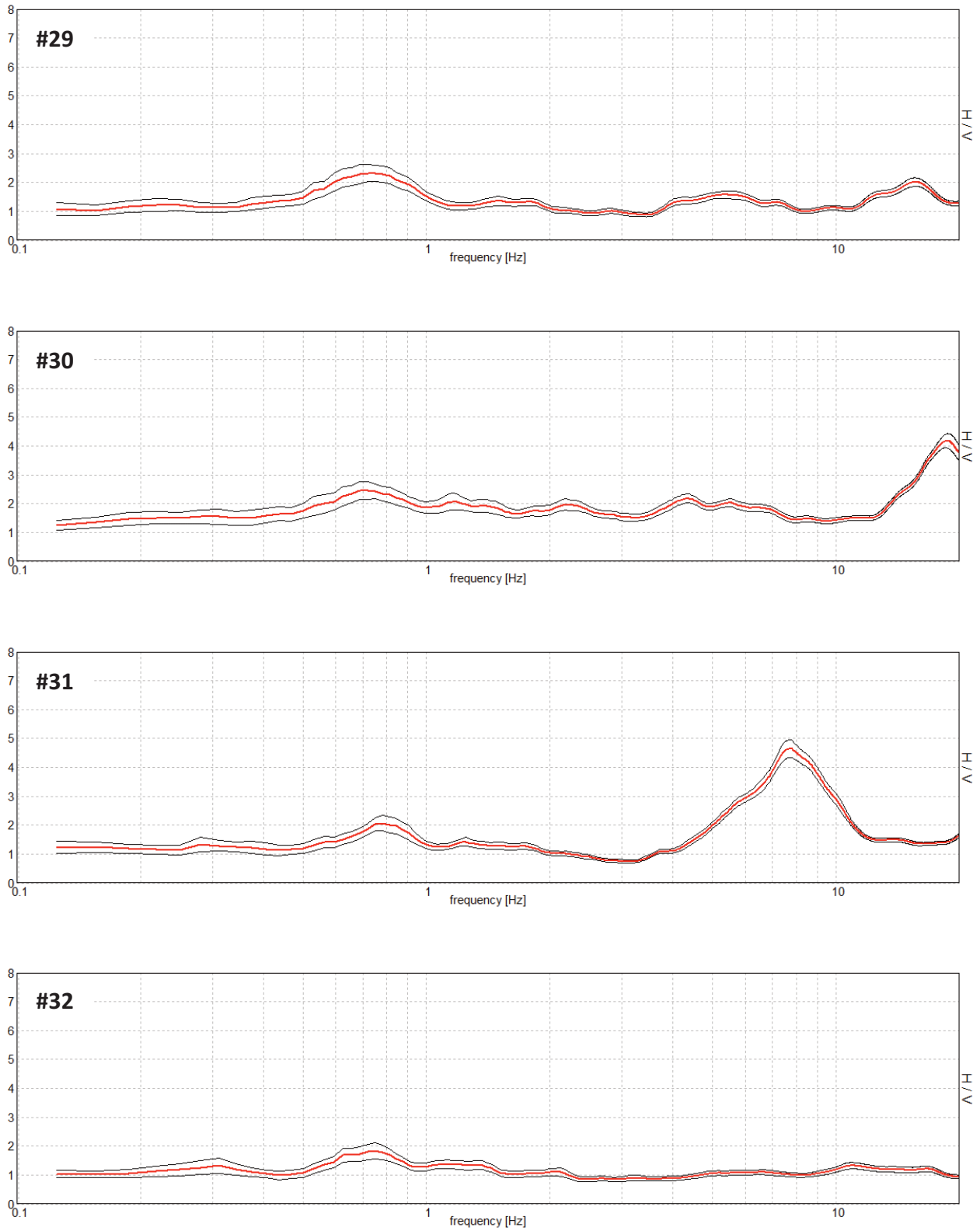


FIGURE S2. HVSR curves relative to the measurement points shown in Figure S1 (#64). Red curve = mean spectral ratio, black curves = standard deviation.

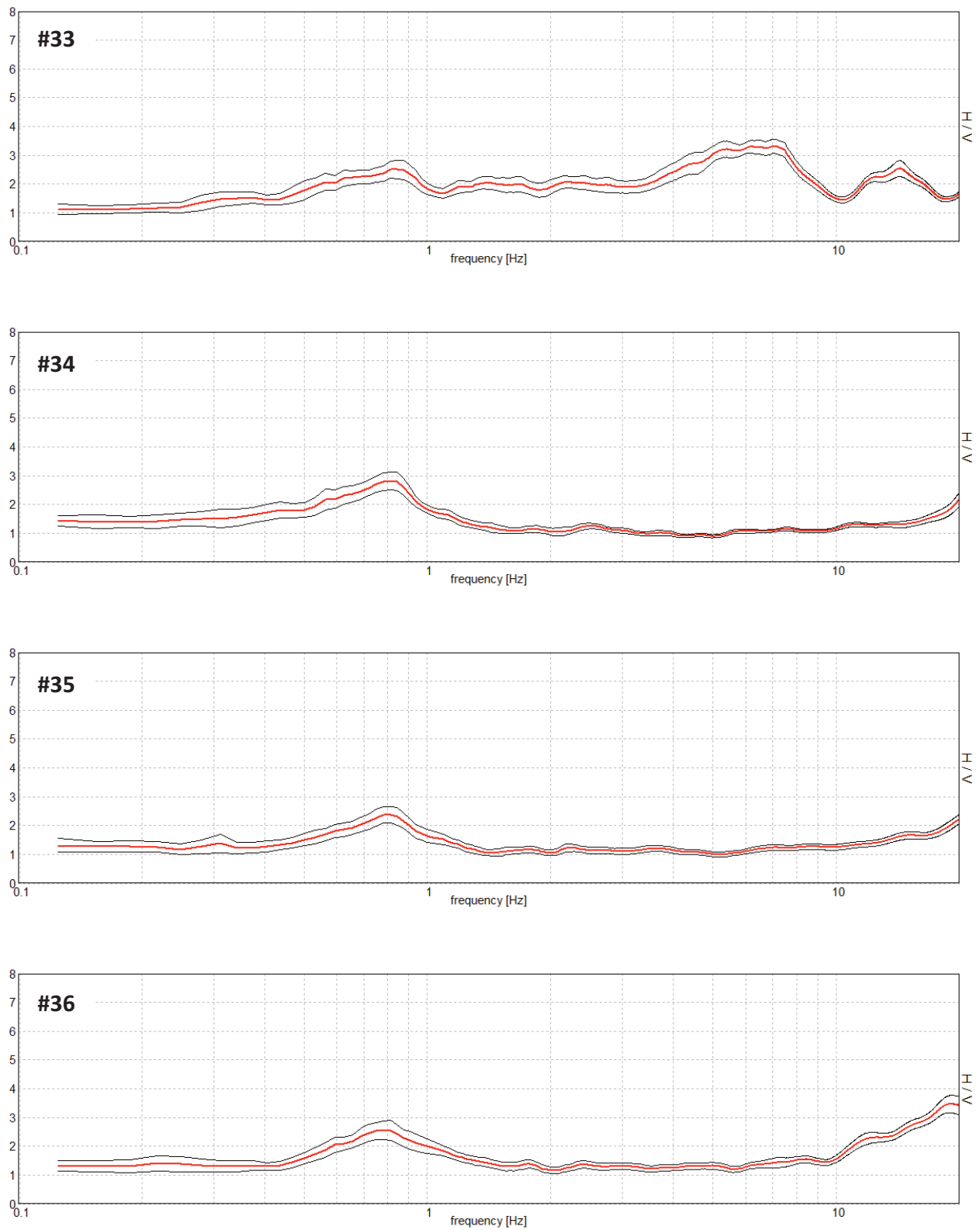


FIGURE S2. HVSR curves relative to the measurement points shown in Figure S1 (#64). Red curve = mean spectral ratio, black curves = standard deviation.

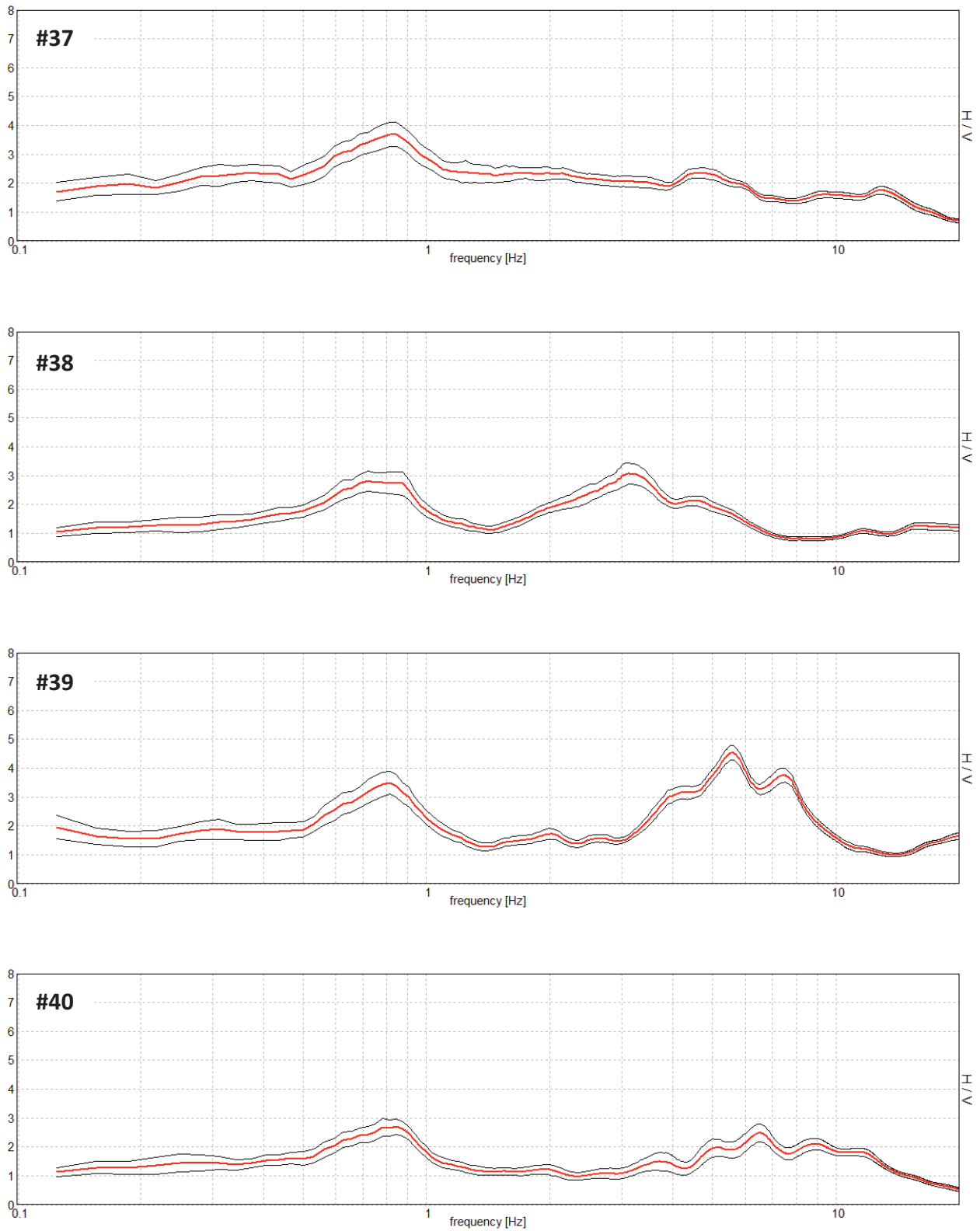


FIGURE S2. HVSR curves relative to the measurement points shown in Figure S1 (#64). Red curve = mean spectral ratio, black curves = standard deviation.

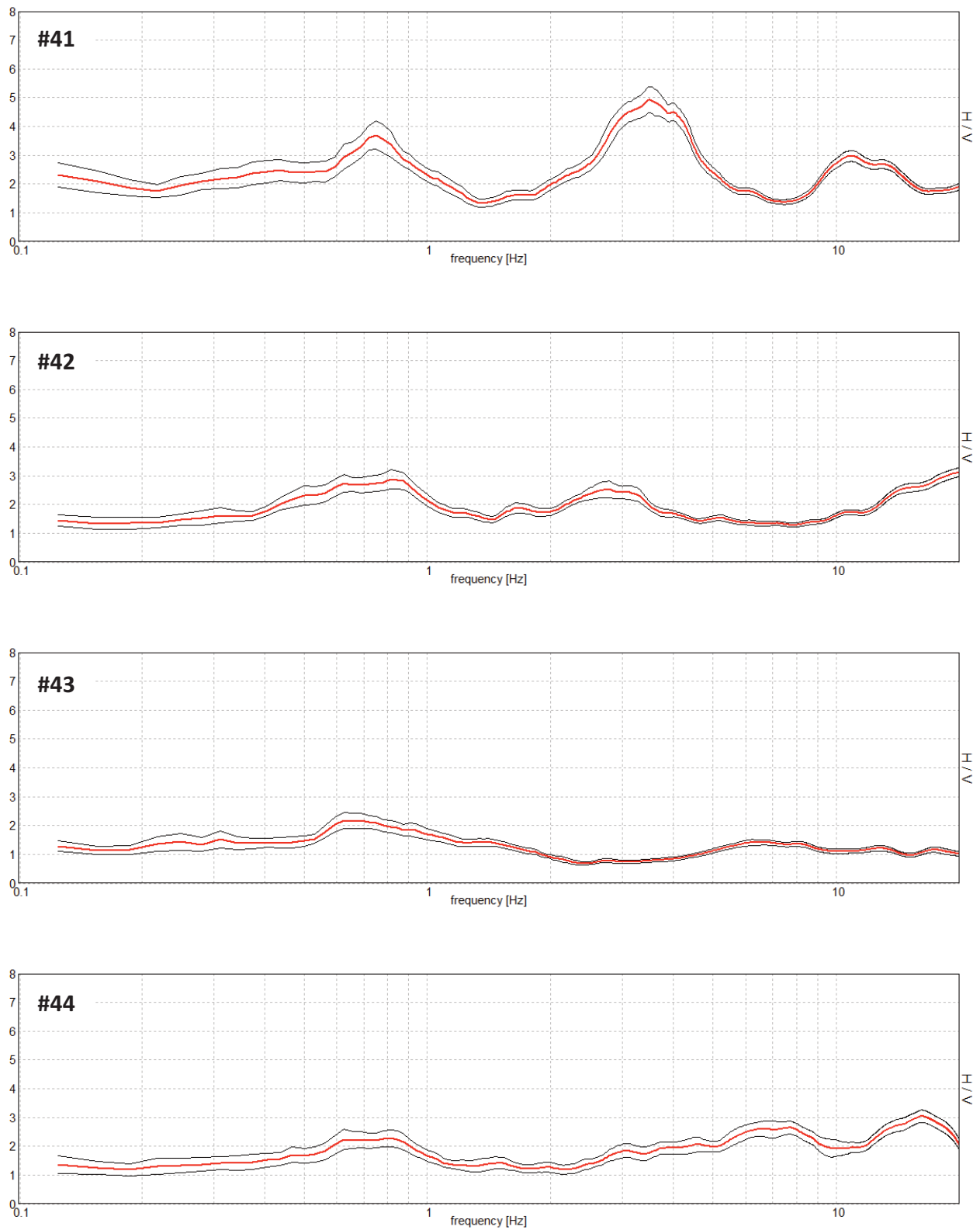


FIGURE S2. HVSR curves relative to the measurement points shown in Figure S1 (#64). Red curve = mean spectral ratio, black curves = standard deviation.

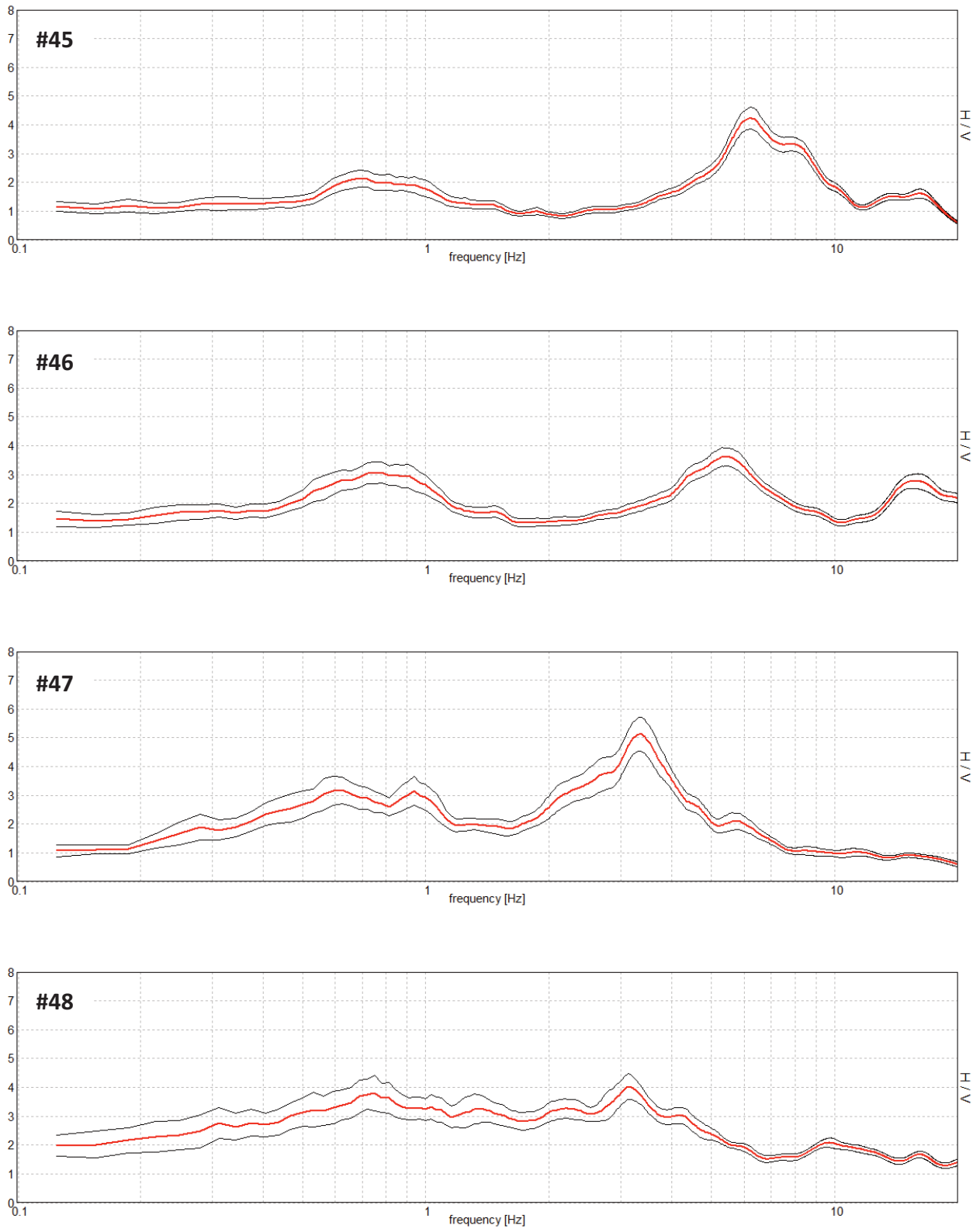


FIGURE S2. HVSR curves relative to the measurement points shown in Figure S1 (#64). Red curve = mean spectral ratio, black curves = standard deviation.

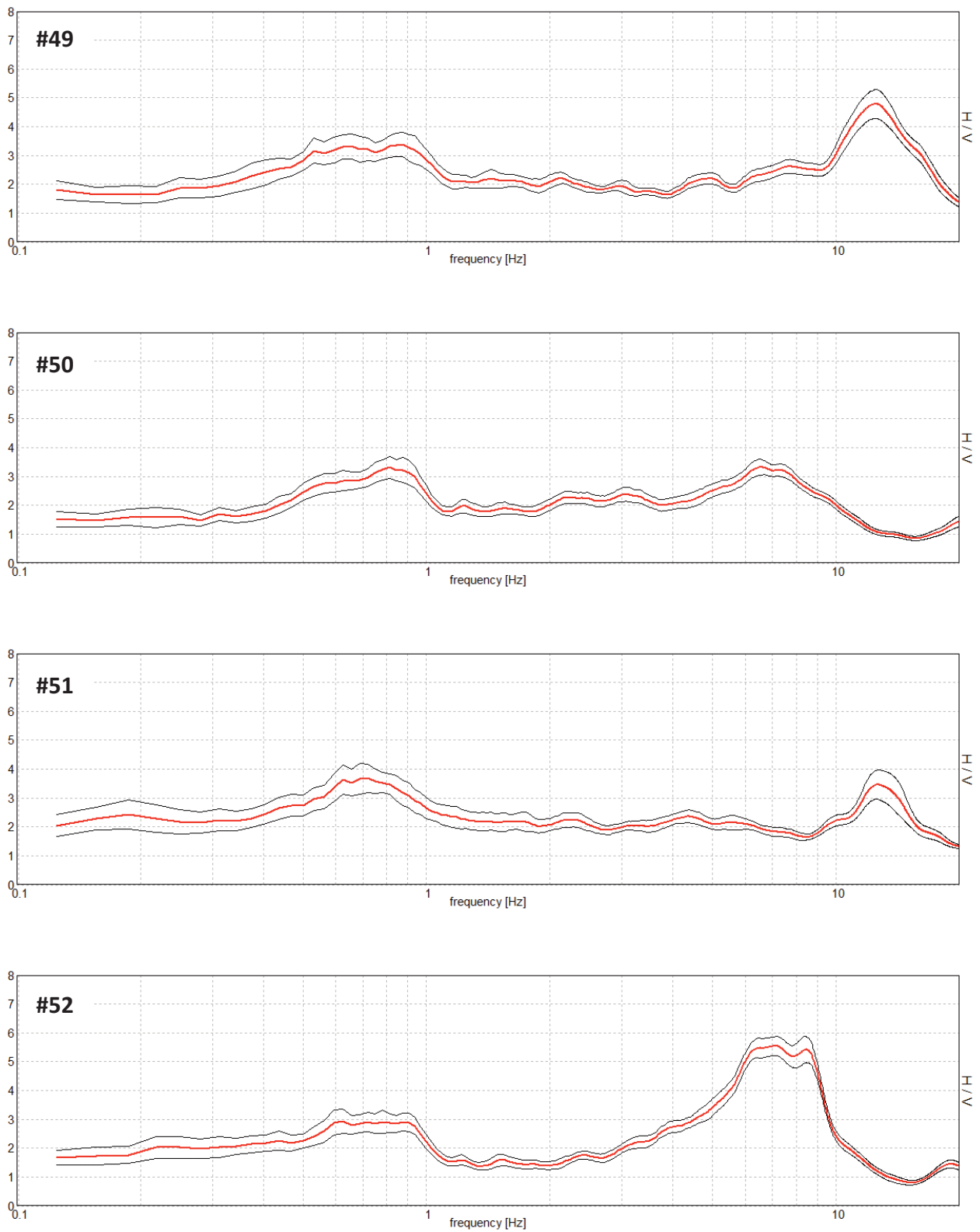


FIGURE S2. HVSR curves relative to the measurement points shown in Figure S1 (#64). Red curve = mean spectral ratio, black curves = standard deviation.

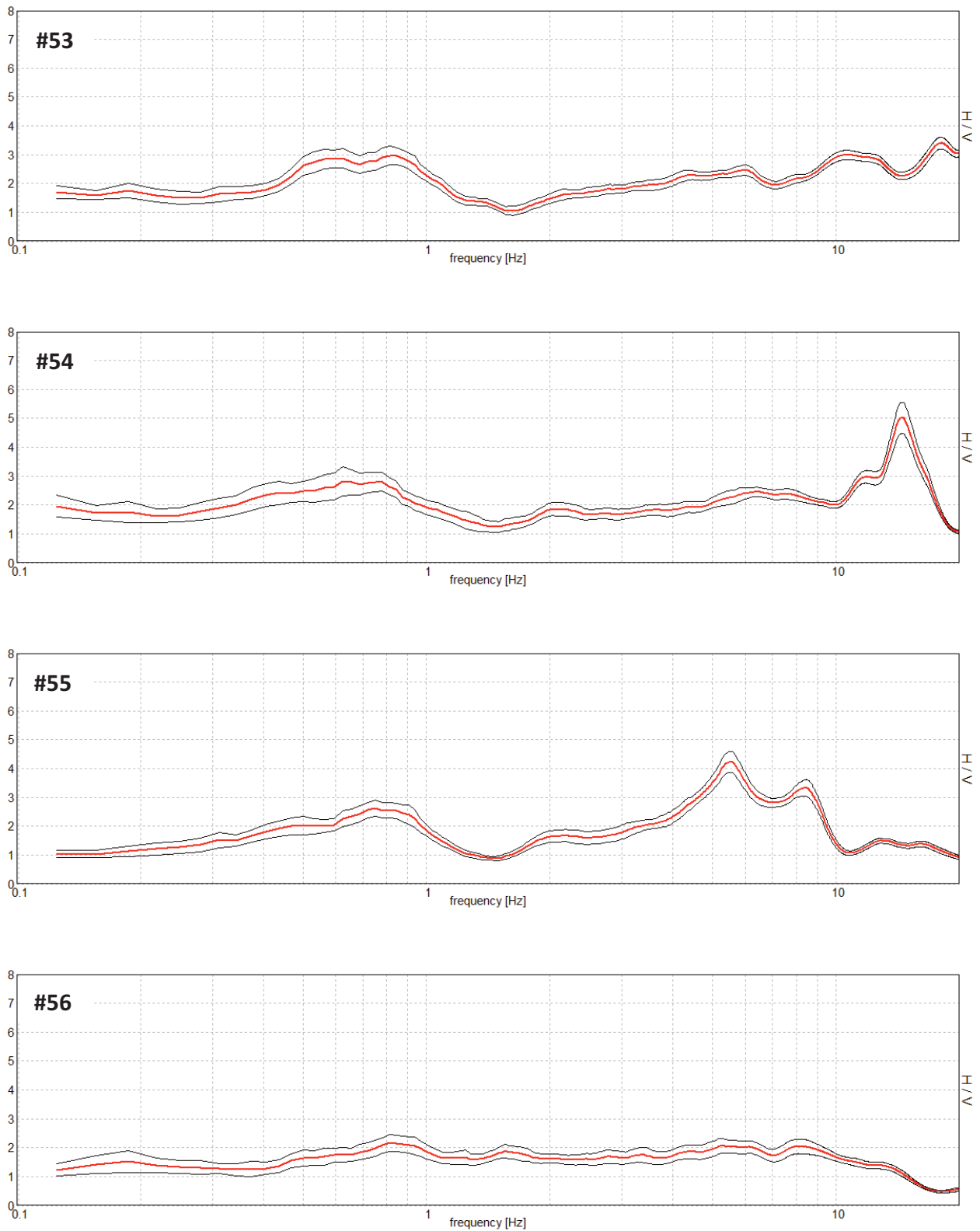


FIGURE S2. HVSR curves relative to the measurement points shown in Figure S1 (#64). Red curve = mean spectral ratio, black curves = standard deviation.

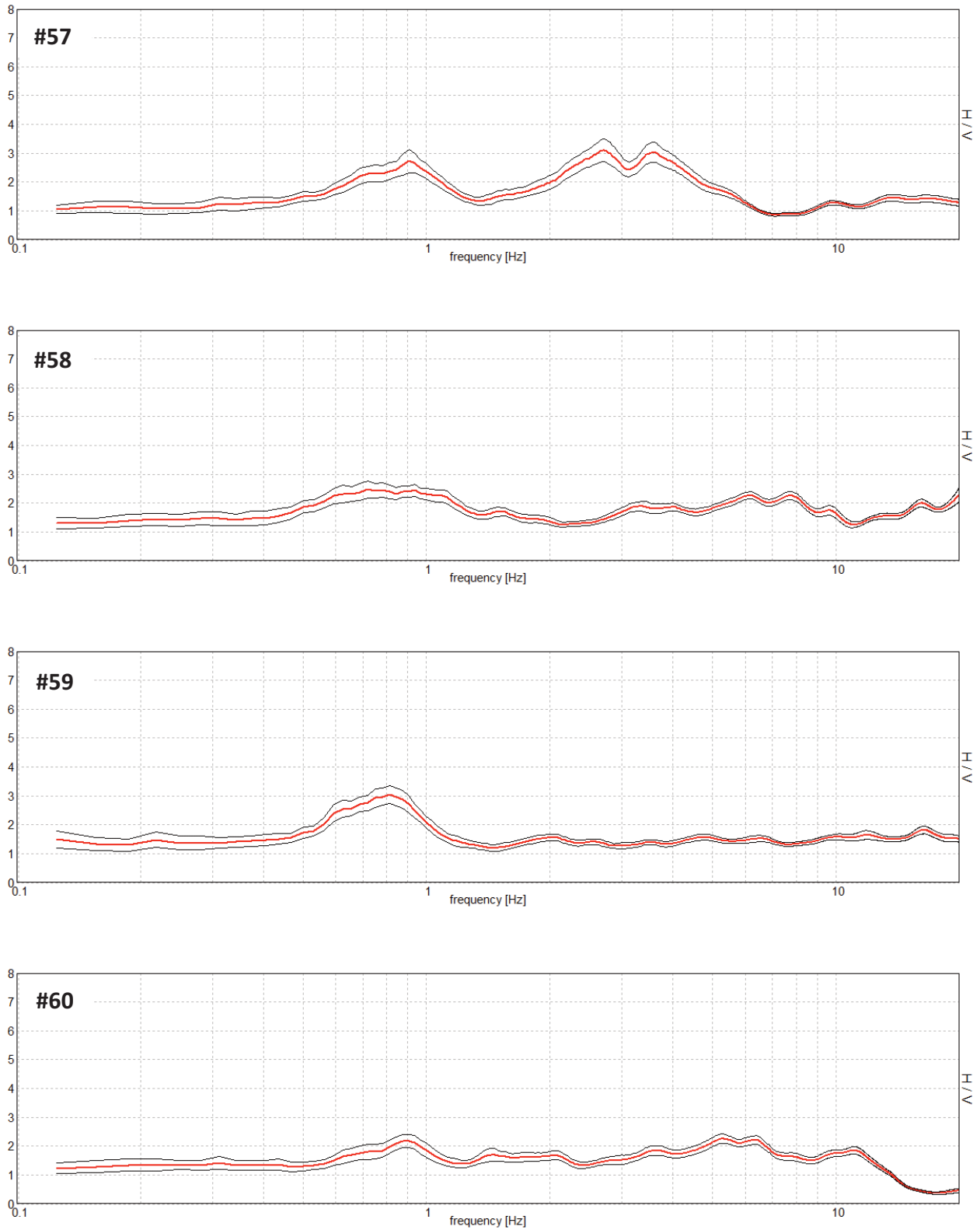


FIGURE S2. HVSR curves relative to the measurement points shown in Figure S1 (#64). Red curve = mean spectral ratio, black curves = standard deviation.

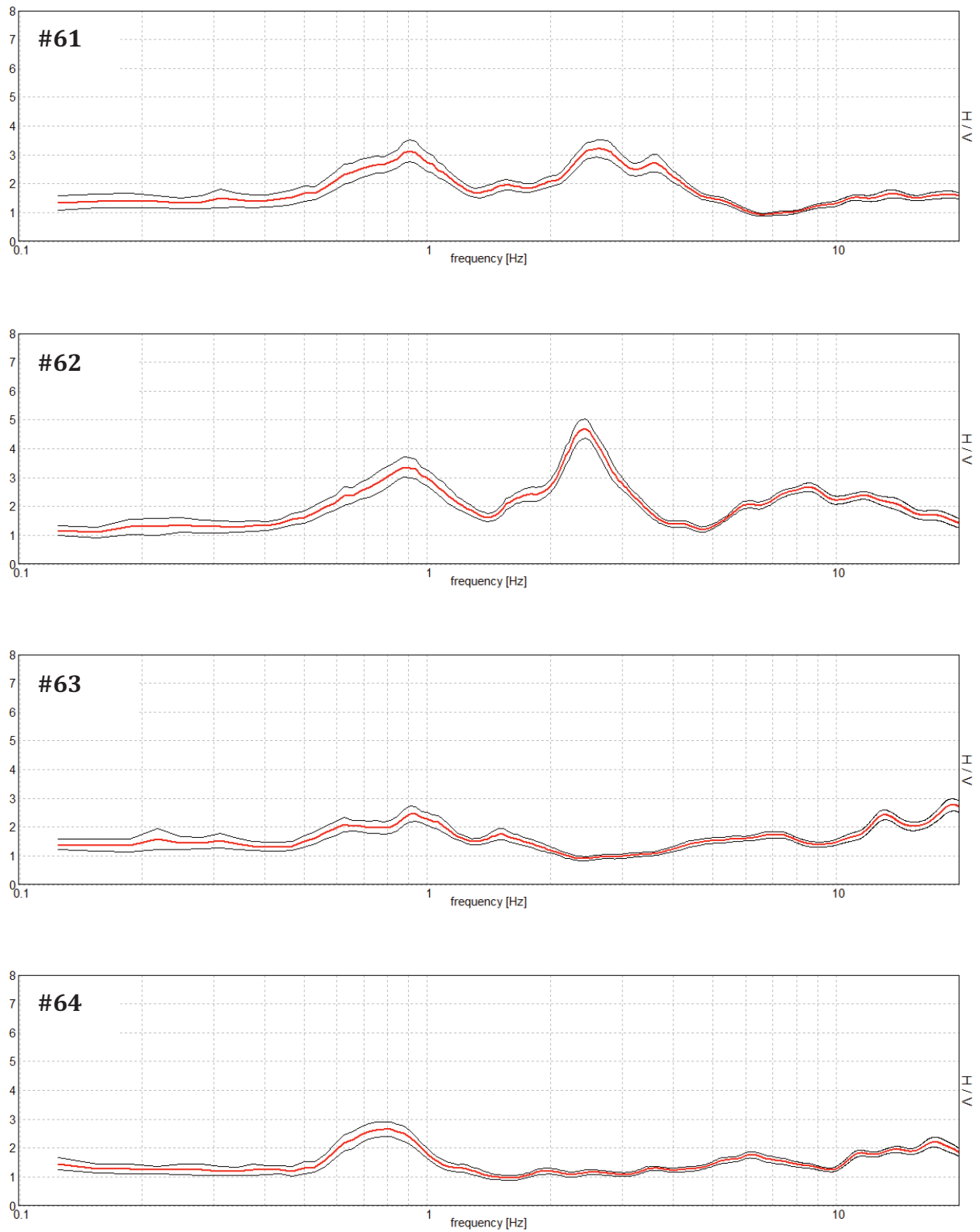


FIGURE S2. HVSR curves relative to the measurement points shown in Figure S1 (#64). Red curve = mean spectral ratio, black curves = standard deviation.